

1 An improved modelling chain for bias-adjusted high-resolution 2 climate and hydrological projections for Norway

3 Shaochun Huang¹, Wai Kwok Wong¹, Andreas Dobler³, Sigrid Jørgensen Bakke¹, Stein Beldring¹,
4 Ingjerd Haddeland^{1*}, Hans Olav Hygen³, Tyge Løvset², Stephanie Mayer², Kjetil Melvold¹, Irene Brox
5 Nilsen¹, Gusong Ruan¹, Silje Lund Sørland^{2^}, Anita Verpe Dyrørdal³

6 ¹Department of Hydrology, Norwegian Water Resources and Energy Directorate, Oslo, 0301, Norway

7 ²NORCE Research AS, and Bjerknes Centre for Climate Research, Bergen, 5008, Norway

8 ³Department of Climate and Environment, Norwegian Meteorological Institute, Oslo, 0371, Norway

9 [^]now at SWECO AS, Bergen, Norway

10 ^{*}now at Lyse AS, Stavanger, 4018, Norway

11 *Correspondence to:* Shaochun Huang (shh@nve.no)

12 **Abstract**

13 About every 10 years, the Norwegian Centre for Climate Services publishes a national climate assessment report, presenting
14 the updated historical climate change and climate projections towards the end of this century. This paper documents the model
15 experiment used to generate high-resolution climate and hydrological projections for the new climate assessment report
16 published in October 2025. The model experiment follows the standard modelling chain for hydrological impact assessment,
17 i.e., climate model selection - downscaling and bias adjustment - hydrological modelling. However, compared with the model
18 experiment for the climate assessment report published in 2015, all modelling components have been improved in terms of
19 data availability, data quality and methodology. Specifically, a large climate model ensemble was available and new criteria
20 were developed to select tailored climate projections for Norway. Two bias-adjustment methods (one univariate and one
21 multivariate) were applied to account for the uncertainty of method choice. The hydrological modelling was improved by
22 implementing a physically-based Penman-Monteith method for evaporation and a glacier model accounting for glacier retreat
23 under climate change scenarios. Besides model description, this paper elaborates the effects of different bias-adjustment
24 methods and the contribution of climate models and bias-adjustment methods to the uncertainty of climate and hydrological
25 projections under the RCP4.5 scenario as examples. The results show that the two bias-adjustment methods can contribute
26 larger uncertainty to seasonal projections than climate models. The multivariate bias-adjustment method improves hydrological
27 simulations, especially in the reference period, but cannot conserve climate change signals of the original climate projections.
28 The dataset generated by the presented modelling chain provides the most updated, comprehensive and detailed
29 hydrometeorological projections for mainland Norway, serving as a knowledge base for climate change adaptation to decision
30 makers at various administrative levels in Norway.

32 **Key words: COR-BA-2025, distHBV-COR-BA-2025, RCP, CORDEX, EQM, 3DBC, distHBV, DEW, NORWAY**

33 **1 Introduction**

34 It is unequivocal that human influence has warmed the climate at a rate that is unprecedented in at least the last 2000 years
35 (IPCC, 2021). The human-induced warming has already modified the global hydrological cycle, leading to significant shifts
36 in the spatial and temporal patterns of hydrological components (Gu and Adler, 2015; Gudmundsson et al., 2021; Li et al.,
37 2023) and more intensive and frequent hydroclimatic extreme events (Alifu et al., 2022; Chinita et al. 2021; Dunn et al., 2020;
38 Padrón et al., 2020). These impacts pose unprecedented challenges for water resource management at regional and local scales,
39 and they are expected to be more severe in the future if unsustainable development continues (Wang and Liu, 2023). Therefore,
40 understanding of the potential climate change impact from a long-term and systematic perspective serves as a key basis to
41 develop climate adaptation strategies, such as incorporating climate projections into European building standards (EEA, 2025)
42 and national climate risk adaptations (DCCEW, 2023).

43 General circulation models (GCMs) are important tools to understand and predict climate behavior under various greenhouse
44 gas emission scenarios on the global scale. GCMs have been developed rapidly in the last decades, with an increasing number
45 of models from over 40 within the Coupled Model Intercomparison Project phase 5 (CMIP5, Taylor et al., 2012) for
46 Representative Concentration Pathway (RCP) emission scenarios to over 60 within CMIP6 (Eyring et al., 2016) for the Shared
47 Socioeconomic Pathways (SSP) emission scenarios. Such a large ensemble of models provides valuable information of
48 uncertainty for future climate projections, accounting for natural climate variability, unknown socio-economic developments,
49 and model differences (Hawkins and Sutton, 2011). However, the use of the full ensemble can be challenging for impact
50 models due to computational restrictions, so it often requires a careful selection of projections for specific study areas based
51 on comprehensive analysis of the whole ensemble (Dalelane et al., 2018). In addition, GCM outputs are hardly applied for
52 impact assessment at regional and local scales due to their coarse spatial resolutions (e.g., ~ 0.25 to 3° for the CMIP6 models
53 and ~ 0.5 to 4° for the CMIP5 models) and systematic biases (Rössler et al., 2019), and they are usually downscaled to fine
54 spatial resolutions and bias adjusted for climate impact assessment and adaptation planning (Martinich & Crimmins, 2019).

55 The GCM outputs can be downscaled dynamically using regional climate models (RCMs) or statistically based on statistical
56 relationships between coarse-resolution variables in GCMs and fine-resolution or local observations in the historical period
57 (Zhang et al., 2020). Various RCMs and statistical downscaling methods have been developed and applied to downscale the
58 GCM outputs, increasing the number of climate projections for region scales. For example, the European Coordinated Regional
59 Downscaling Experiment (EURO-CORDEX, Jacob et al., 2020) applies 11 RCMs to downscale the outputs from 14 GCMs to
60 0.11° (ca. 12.5 km) horizontal resolution. Due to the high computational cost and time consumption, each RCM is able to
61 downscale one or a few GCMs outputs, resulting in 30, 25 and 64 regional climate projections for Europe under the RCP2.6,
62 RCP4.5 and RCP8.5 scenarios, respectively. In contrast, statistical downscaling methods, which are often combined with bias

63 adjustment, can be easily applied for a large ensemble of GCMs due to low computational requirements and fast calculations,
64 and over 50 statistical downscaling methods have been applied for Europe (Gutiérrez et al., 2019).

65 Each downscaling method has its strengths and weaknesses. The dynamic downscaling ensures the physical relationships
66 between climatic variables and spatial dependence, but it inherits significant biases from GCMs and requires further bias
67 adjustment and/or statistical downscaling depending on the scale of impact studies (Hundecha et al., 2016; Maraun og
68 Widmann, 2018). In contrast, the statistical downscaling usually outperforms the RCMs in terms of bias, but many methods
69 downscale individual climatic variables independently. ~~(univariate) and As univariate bias-adjustment methods, this approach~~
70 ~~does not modify ean lead to inaeccurate~~ inter-variable dependency structures but keeps them as in the original model data which
71 ~~can be inaccurate~~. Eum et al. (2020) demonstrated ~~substantial-different~~ impact of ~~the~~-univariate and multivariate statistical
72 downscaling methods on reproduction of snowfall and recommended the use of the multivariate methods for climate change
73 impact assessment in snow-dominated watersheds. Meyer et al. (2019) also found underestimation of snow accumulation (up
74 to 50%) in alpine catchments when using univariate contra multivariate bias-adjustment approach, which can be attributed to
75 less precipitation below temperatures of 0 °C.

76 Due to the large number of GCM projections and downscaling methods, as well as their strengths and weaknesses, to construct
77 a downscaled and bias-corrected ensemble for specific regions is challenging. Different choices of GCM and downscaling
78 methods can lead to considerably different local climate projections and thus contribute large uncertainty to local decision-
79 relevant climate outcomes (Tang et al., 2016; Lafferty & Sriver, 2023). In addition, they result in different climate impact
80 projections for streamflow (K~~ae~~y, ~~2022~~2025), flood hazard (Kundzewicz et al., 2017), agriculture (Li et al., 2023), ecosystem
81 (Pourmokhtarian et al., 2016), etc, causing inconsistent impact assessments not only within each impact sector but also across
82 sectors. Therefore, a consistent and tailored ensemble of regional climate projections is highly appreciated for each region and
83 many countries have put great efforts to create national ensembles of climate projections (Golding et al., 2025), such as
84 Switzerland (Fischer et al., 2022), Germany (Hübener et al., 2017), UK (Reyniers et al., 2025) and Australia (Peter et al.,
85 2024).

86 Norway is located in the northern high latitudes, which have experienced the strongest warming since 1980 among all regions
87 in the world, with warming trends spanning from 0.2 to more than 0.6 °C/decade (IPCC, 2021). The strong warming in the
88 historical period raises great attention from both the scientific community and the public to future climate change and its
89 impacts on hydropower production (about 90% of total power production in the country), winter tourism (skiing), and water
90 related natural hazards (i.e., flood, drought, avalanche and landslide). However, it is specifically challenging to construct robust
91 and reliable climate projections as well as hydrological impact projections in Norway, due to the high heterogeneity in
92 topographic and hydroclimatological characteristics.

93 Norway is one of the most mountainous countries in Europe, with more than 90% of the landscape consisting of mountains.
94 The rugged topography leads to a complex spatial and temporal pattern of temperature and precipitation, varying with
95 geographical position, elevation, aspect (slope direction), and slope angle (Dobrowski et al., 2009; Franke, 2024). The spatial
96 resolutions of the state-of-the-art GCMs and RCMs are too coarse to provide sufficient spatial variations of climate for such
97 complex terrain. In addition, these projections often show a cold bias for Norway (Wong et al., 2016), which for example leads
98 to a prolonged snow season, low winter runoff and late snowmelt in hydrological projections (Nilsen et al., 2021).

99 In order to construct a consistent and tailored ensemble of national climate projections as well as hydrological projections for
100 Norway, the Norwegian Centre for Climate Services (NCCS) brings together experts from the Norwegian Meteorological
101 Institute, the Norwegian Water Resources and Energy Directorate (NVE), the Norwegian Research Centre (NORCE) and
102 Bjerknæs Centre for Climate Research. NCCS is responsible for the national climate assessment report, updated about every
103 10 years, which presents updated historical climate change and climate projections towards the end of this century and serves
104 as a knowledge base for climate change adaptation to decision makers and planners at various administrative levels in Norway
105 (Nilsen et al., 2022). The previous climate assessment report “Climate in Norway 2100” (Hanssen-Bauer et al., 2015; hereafter
106 abbreviated CiN-2015), published in 2015, was based on 10 available GCM-RCM combinations within the CMIP5 and EURO-
107 CORDEX frameworks. The projections were further re-gridded and bias-adjusted into 1×1 km resolution using empirical
108 quantile mapping and forced the distributed version of the HBV (Hydrologiska Byråns Vattenbalansavdelningen, i.e. “The
109 Hydrological Bureau’s Water Balance Department”) hydrological model (distHBV, Beldring et al., 2003) to generate
110 hydrological projections. This spatial resolution is the result of the need to serve projections that can be used locally on the
111 one hand, and availability of computational resources and reference datasets to produce daily maps for the whole of Norway
112 on the other. During the last 10 years, all methods along the modelling chain, including GCMs, RCMs, climate model
113 selections, statistical downscaling and bias correction, and hydrological models, have been further developed, and the
114 observation data has been updated and improved. These developments promote the new generation of high-resolution and
115 bias-adjusted climate and hydrological projections, which are more robust than the previous ones in CiN-2015.

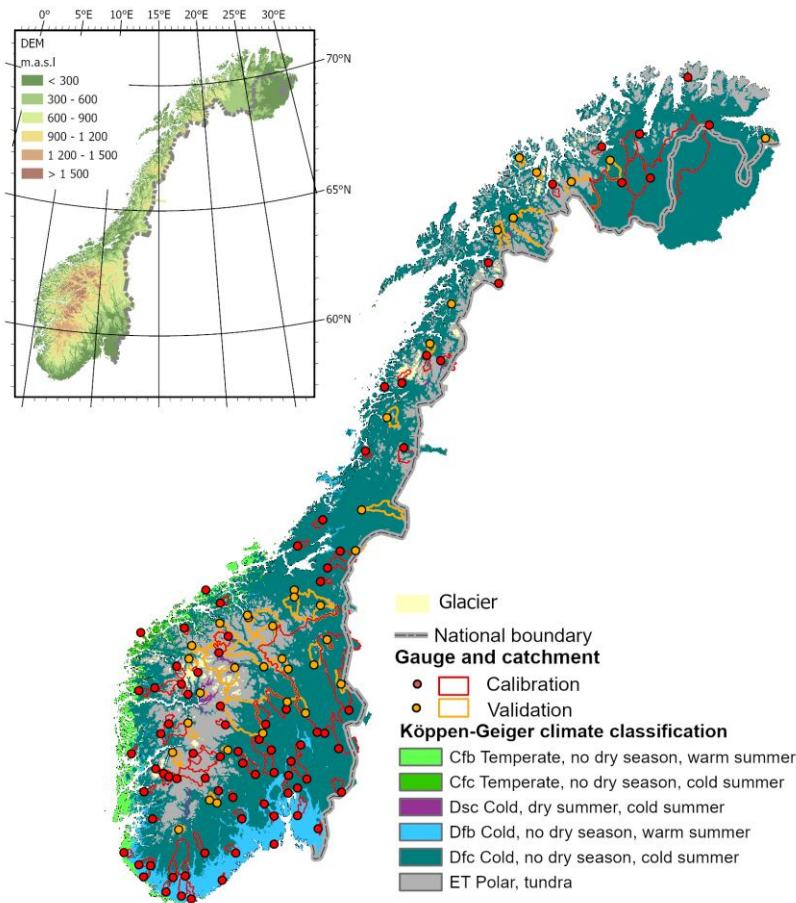
116 In this paper, we present the full description of the methods to produce the updated downscaled and bias-adjusted climate
117 projections and hydrological projections for the new climate assessment report for Norway “CiN-2025” (Dyrredal et al., 2025),
118 specifically focusing on selection of GCM-RCMs combinations, statistical downscaling and bias-adjustment and hydrological
119 modelling. Section 2 introduces the study area and historical input data. The methods described include the overview of the
120 whole modelling chain (Section 3), selection of atmospheric variables from a set of EURO-CORDEX simulations (Section 4),
121 statistical downscaling and bias-adjustment method (Section 5) and hydrological modelling (Section 6). In Section 7 and 8,
122 we present the climate and hydrological products and uncertainty analysis. Finally, we discuss the limitations of the methods
123 and the potential applications of the products, and point out the way towards the next generation of national climate projections
124 for Norway in Section 9.

125 2 Study area and historical data

126 2.1 Study area

127 The modelling domain of this study is the mainland of Norway and a few river catchments draining from neighbouring
128 countries (Sweden and Finland) (Fig. 1), resulting in 354448 1x1 km² grid cells. Due to large variations in latitude and altitude,
129 Norway exhibits six climate regimes according to the Köppen-Geiger climate classification (Beck et al., 2018), ranging from
130 temperate climate along the west coast to polar climate in high mountains and in the north (Fig. 1). The average elevation of
131 Norway is about 460 m, ranging from 0 along the coast to 2469 m at Galdhøpiggen in the center of the country. Open firm
132 ground and forest are the two major land covers in Norway, accounting for 36% and 37.8% of the mainland area, respectively
133 (Statistics Norway, 2025). There are also large areas of bedrock (8.5%), followed by water (6.2%), bogs (5.4%), agricultural
134 land (3.5%) and built-up (1.7%). About 1% of mainland Norway is covered by glaciers (Fig. 1). The mean annual temperature
135 in the current standard normal period 1991–2020 ranges from -9.5 to +9.5 °C (Tveito, 2021). The warmest areas are found in
136 lower-lying areas in southern Norway, and particularly along the coast in the southwest, while the coldest areas are in the high
137 mountains and inland areas of the north. Norway also exhibits large spatial variability in precipitation, ranging from 212 mm
138 in southern parts of Northern Norway to 6130 mm close to the Ålfotbreen glacier in Western Norway. The wet areas along the
139 west coast are exposed to migrating low pressure systems most often arriving from the west-southwest (Lutz et al., 2024).

140 We selected 85 and 38 catchments for calibration and validation of the hydrological model, respectively. All these catchments
141 are near-natural catchments and 112 of the 123 catchments are smaller than 1000 km². The distribution of the catchments
142 represents various climate and hydrological regimes, geographic conditions and landscape types in Norway. The catchment
143 boundary is delineated by NVE and the gauges at the outlet of these catchments are shown in Fig. 1.



144

145 **Figure 1: the climatic and topographic characteristics of the simulation domain as well as the locations of glaciers and hydrological**
 146 **gauging stations and catchment boundaries.**

147 **2.2 Historical meteorological data**

148 The historical meteorological data is used as reference in the bias-adjustment procedures and for hydrological model calibration
149 and validations. It consists of nine atmospheric meteorological variables at a 1 x 1 km² grid covering Norway and river
150 catchments in neighbouring countries (Fig. 1): mean, minimum and maximum 2m temperature (K), precipitation flux (mm/s),
151 relative humidity (%), longwave and shortwave radiation (W/m²), pressure (Pa) and 10m wind speed (m/s).

152 Daily minimum, maximum and mean temperatures as well as precipitation are provided by the seNorge2018 v20.05 dataset
153 (Lussana et al., 2019; 2020). It covers the period 1957–2020 and is based on quality-assured daily datasets. The precipitation
154 values are adjusted for wind-induced under-catch based on Wolff et al. (2015). Note that seNorge2018 continuously
155 incorporates the latest available station data and is therefore not homogenized in time. This may affect the calculation of
156 changes within the historical period.

157 Daily wind speeds for Norway from 1958 to 2020 are obtained from the KliNoGrid 16.12 dataset. The KliNoGrid dataset is
158 based on the Norwegian atmospheric reanalysis NORA10 (Reistad et al., 2011) wind speed data, downscaled onto a 1 km grid
159 using a quantile mapping approach (Bremnes, 2004) to match the climatology of the high-resolution numerical weather
160 prediction model AROME-METCoOp (Müller et al., 2017).

161 Daily short- and longwave radiation, relative humidity and surface pressure are obtained from the HySN2018v2005ERA5
162 dataset. It is generated based on the ECMWF atmospheric reanalysis ERA5 (Hershebach et al., 2020+8) and seNorge2018
163 v20.05 and covers the period 1958–2020. The dataset is described in detail in Huang et al. (2022) and Erlandsen et al. (2021).

164 **2.3 Data for setting-up hydrological models**

165 To set up the hydrological model, a digital elevation model (DEM), as well as maps of soil type and land cover type with 1
166 km horizontal resolution are required. The DEM map was provided by the Norwegian Mapping Authority. Five soil types are
167 reclassified based on the sediment map from the Geological Survey of Norway (Erlandsen et al., 2021), and bare mountain
168 soil and moraine soils account for ca. 80% of the total mainland area. Nine land cover types (open area, bog, built-up, forest,
169 cropland, heather, bedrock, lake, permanent ice and snow) are classified based on the National Land Resource Map (Ahlström
170 et al., 2014) and the remote sensing based forest resource map SAT-SKOG (Gjertsen and Nilsen, 2012). The forest land cover
171 is further classified into 12 structural forest types to distinguish three species groups (spruce, pine, and deciduous forest) and
172 four forest development stages (underdevelopment, two intermediate development stages and mature forest) (Majasalmi et al.,
173 2018). The parametrization for each forest structural type, such as maximum leaf area index, vegetation height and shortwave
174 albedo, is given by Majasalmi et al. (2018) and Bright et al. (2018). For glacier areas, the glacier modelling doesn't account
175 for variation of soil types and uses simplified land cover types including open area, bog, forest, bedrock and glacier area
176 coverage. However, it requires glacier ice thickness and glacier area data (Andreassen et al. 2015) to setup the model.

177 Discharge measurements from 123 gauging stations are used to calibrate and validate the hydrological model (Fig. 1). They
178 are quality-assured by NVE. All 123 stations have measured daily discharge from 1980 to 2014 with less than 5% missing
179 data. For the glacier modelling, mass balance data is only available for six glaciers and discharge measurements from 19
180 gauging stations downstream of the glaciers are used to calibrate and validate the hydrological model. All discharge and mass
181 balance data are publicly available at sildre.nve.no and glacier.nve.no/glacier/viewer/ci/en/.

182 **3 Modelling chain**

183 We followed the commonly used modelling chain in hydrological climate impact studies, i.e., 1) emission scenarios, 2) GCMs
184 and RCMs, 3) statistical downscaling and bias correction and 4) hydrological model (Fig. 2). The first component of the
185 modelling chain is to select emission scenarios. For the CiN-2025 report, two RCPs used in CMIP5 were selected, representing
186 a very stringent pathway (RCP2.6) and a moderate-emissions pathway (RCP4.5). The shared socioeconomic pathway SSP3-
187 7.0 used in CMIP6 was selected to represent the high-emission scenario. The reason why only one SSP scenario was selected
188 is that SSP1-2.6 and SSP3-7.0 were the first-priority scenarios for the EURO-CORDEX community (Katragkou et al., 2024).
189 The data has become available late with regard to the time needed to run our complete modelling chain - it is in fact still not
190 openly available - making the selection of more than one SSP scenario infeasible. Such a combination of CMIP5 and CMIP6
191 scenarios has also been used in other national climate projections, e.g., the climate projections in Switzerland published at the
192 end of 2025 (Schumacher et al., 2024) which combined EURO-CORDEX RCP8.5 with CMIP6 SSP5-8.5 GCM simulations.

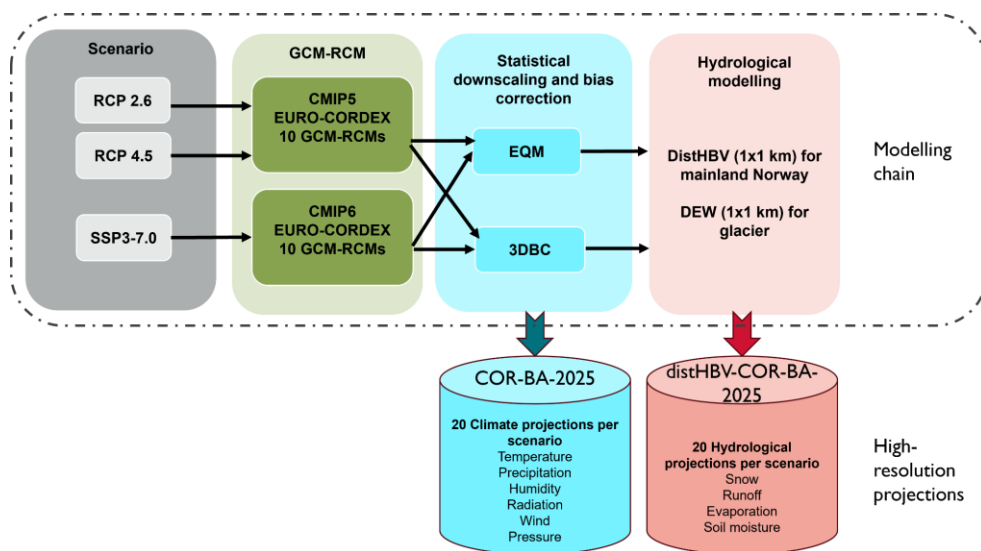


Figure 2: Modelling chain to generate high-resolution climate and hydrological projections for the CiN-2025 report.

In the second component of the modelling chain the task is to select a representative model ensemble from the EURO-CORDEX simulations (Jacob et al., 2014) for each emission scenario. Within the EURO-CORDEX framework, CMIP5 and CMIP6 GCMs are downscaled by different RCMs, resulting in a set of GCM-RCM combinations. For CiN-2025 a larger EURO-CORDEX ensemble for RCP scenarios was available compared to CiN-2015, enabling a more robust data basis and requiring new model selection strategies (Section 4).

Once the model ensemble was identified, the next step was to downscale the RCM projections of atmospheric variables from the original grid size of approximately 12.5 km to 1 km. It was followed by removal of biases in RCM simulations relative to observed meteorological data (Section 2.2) in the calibration period. For future projections, we adjusted the values based on the corrections established in the calibration period under the assumption that the relationship between the observed and modelled data remains unchanged. Two bias-adjustment methods were used: de-trended empirical quantile mapping (denoted as EQM hereafter for simplicity) and three-dimensional bias-correction (3DBC) additionally to EQM (Section 5). The former is a widely used univariate bias-adjustment method and was used for CiN-2015. The latter adds a post-processing procedure, taking into account inter-variable dependencies. To our knowledge, this is the first time the 3DBC method is applied in Norway, and we have identified several strengths and weaknesses with this multivariate method (Section 5.3). Since the two bias-adjustment methods complement each other, we decided to apply both bias-adjustment methods on the RCM projections

210 and provided two complete datasets (EQM only and EQM with 3DBC). To assess the uncertainty in the climate and
211 hydrological projections from the choice of methods, we have carried out an uncertainty analysis (Section 7.3 and 8.3).

212 The last component of the modelling chain is hydrological modelling. The distHBV model was still the main tool for simulating
213 hydrological components under different climate scenarios for the CiN-2025 report, but two major improvements have been
214 made since CiN-2015. The first improvement was to replace the temperature-based evaporation method with the Penman-
215 Monteith equation in the distHBV model (Huang et al., 2019), because physical-based approaches, such as the Penman-
216 Monteith method, consider more climatic variables and provide more robust changes in potential evaporation under climate
217 scenarios than the empirical ones (McAfee, 2013; Tam et al., 2024). The second improvement was ~~the inclusion of the use of~~
218 Distributed Element Water balance model (DEW) (Beldring, 2008) ~~for glacierized regions, which is an advanced version of~~
219 ~~distHBV in terms of the glacier module~~. Since distHBV was not able to simulate the changes in glacier area, glacier melt water
220 can be unrealistically ~~high-simulated~~ under climate scenarios ~~used in CiN-2015~~. In contrast, DEW is able to simulate glacier
221 area, volume and surface elevation dynamically and thus gives more reliable hydrological projections under climate change
222 for glacierized regions. Both models ran ~~independently~~ at 1 km spatial resolution and with daily time steps, but distHBV ran
223 for all grid cells in Norway and DEW only ran for the grid cells covering glacierized regions. ~~A postprocessing procedure was~~
224 ~~carried out to combine the distHBV and DEW outputs to generate final runoff projections for mainland Norway. The smallest~~
225 ~~glaciers (< 1 km²) were omitted in the DEW model.~~

226 The modelling chain resulted in two datasets with a spatial resolution of 1x1 km at daily time steps, which will be serving as
227 the basis for climate impact assessment in mainland Norway. The first dataset is termed COR-BA-2025 (short for CORDEX-
228 Bias Adjusted, updated in 2025), consisting of 20 bias-adjusted high-resolution climate projections for each emission scenario
229 and is available from 1970 to 2100 (2098 depending on GCMs). These projections include nine atmospheric variables at 1x1
230 km spatial resolution and with daily time steps, ~~each bias-adjusted both with EQM and 3DBC~~: mean, minimum and maximum
231 2m temperature (K), precipitation flux (mm/s), relative humidity (%), longwave and shortwave radiation (W/m²), surface air
232 pressure (Pa) and 10m wind speed (m/s). The second dataset is called distHBV-COR-BA-2025 and consists of 20 hydrological
233 projections for each emission scenario at the same spatial and temporal resolution and coverage as the atmospheric projections.
234 The hydrological projections include two flux variables (runoff and evaporation) representing average values over each grid
235 cell in mm/day, and two state variables (soil moisture and snow water equivalent), which describe the average condition of the
236 hydrological components in a grid cell with unit mm. The evaporation, soil moisture and snow water equivalent projections
237 were generated by distHBV, whereas the runoff projections were obtained by superimposing the results of the glacierized grid
238 cells from the DEW model on the runoff projections from distHBV.

239 To select the climate ensembles and assess future changes in climate and hydrology, we defined one reference period (1991–
240 2020) and two future periods (2041–2070 and 2071–2100). The reference period was selected by two factors: 1) a recent
241 climate period better represents today's climate, and 2) 1991–2020 is the current standard normal period defined by the World

242 Meteorological Organization (WMO). However, in CMIP5 and CMIP6, the historical simulation runs end in 2005 and 2014,
 243 respectively. Data from the emission scenario RCP4.5 was used to extend the historical period beyond 2005 for RCPs and the
 244 data from the emission scenario SSP3-7.0 was used to extend the historical period beyond 2014 for SSPs.

245 Since the main focus of this paper is on the description of the methods in the modelling chain rather than assessing climate
 246 and hydrological projections under different emission scenarios, we ~~only-mainly~~ present the methods and results for the
 247 RCP4.5 scenario as examples in the following sections. However, the methods described in this paper are valid for all three
 248 scenarios.

249 **4 Selection of GCM-RCM combinations**

250 Currently, the EURO-CORDEX CMIP5 projections comprise the largest high-resolution regional climate model ensemble for
 251 Europe and Norway with more than 30 simulations based on RCP2.6, more than 20 simulations based on RCP4.5 and more
 252 than 70 simulations based on RCP8.5. However, there are (only) 17 identical model combinations based on the
 253 representative concentration pathways RCP2.6, RCP4.5 and RCP8.5 covering all three RCPs (Table 1). To be able to do a
 254 proper comparison between future projections of different RCPs, it is important to use identical model combinations for each
 255 RCP. These identical model combinations comprise five GCMs, namely CNRM_CM5, EC_EARTH, HadGEM2-ES, MPI-
 256 ESM-LR and NorESM1-M. Based on all 17 models for RCP4.5, the projected temperature and precipitation changes in Norway
 257 ranges from 0.5 to 3.4 °C and from -2.6 to 12.5 % (indicated as grey shaded area in Fig. 3), respectively. Given time and
 258 computational constraints, we defined an upper limit of ten model combinations that are used as forcing data for the
 259 hydrological models, thus seven model combinations had to be excluded.

260 **Table 1. Summary of the 17 GCM-RCM combinations available for RCP2.6, RCP4.5 and RCP8.5. Combinations in bold were**
 261 **selected for downscaling and bias-adjustment for the mainland of Norway. ¹: Original data has 360 days only. Additional days added,**
 262 **²: Leap-year days added. ³: Spatial smoothing applied to tasmin, tasmax, tas and hurs.**

<u>Model combination name</u>	<u>GCM modelling institute</u>	<u>GCM</u>	<u>RCM modelling institute</u>	<u>RCM</u>	<u>Data coverage</u>
cnrm-r1i1p1-aladin	CNRM-CERFACS	CNRM-CM5	CNRM	ALADIN63	1951-2100
ecearth-r12i1p1-rca³	ICHEC	EC-EARTH	SMHI	RCA4	1970-2100
ecearth-r12i1p1-cclm	ICHEC	EC-EARTH	BTU & KIT (CLMcom)	CCLM4-8-17	1950-2100
ecearth-r3i1p1-hirham³	ICHEC	EC-EARTH	DMI	HIRHAM5	1951-2100

Formatert tabell

hadgem-riilpl-rca^{1,3}	MOHC	HadGEM2-ES	SMHI	RCA4	1970–2098
hadgem-riilpl-remo¹	MOHC	HadGEM2-ES	GERICS	REMO2015	1950–2098
mpi-riilpl-cclm	MPI-M	MPI-ESM-LR	BTU (CLMcom)	CCLM4-8-17	1950–2100
mpi-r2ilpl-remo	MPI-M	MPI-ESM-LR	MPI-CSC	REMO2009	1951–2100
noresm-riilpl-rca^{2,3}	NCC	NorESM1-M	SMHI	RCA4	1970–2100
noresm-riilpl-remo	NCC	NorESM1-M	GERICS	REMO2015	1950–2100
cnrm_rliilpl_alaro	CNRM-CERFACS	CNRM-CM5	RMIB-UGent	ALARO-0	1950–2100
cnrm_rliilpl_racmo	CNRM-CERFACS	CNRM-CM5	KNMI	RACMO22E	1950–2100
gcearth-r12ilpl_racmo	ICHEC	EC-EARTH	KNMI	RACMO22E	1950–2100
gcearth_r12ilpl_remo	ICHEC	EC-EARTH	GERICS	REMO2015	1950–2100
hadgem_rliilpl_racmo¹	MOHC	HadGEM2-ES	KNMI	RACMO22E	1950–2098
hadgem_rliilpl_hirham¹	MOHC	HadGEM2-ES	DMI	HIRHAM5	1951–2098
mpi_rliilpl_remo	MPI-M	MPI-ESM-LR	MPI-CSC	REMO2009	1951–2100

formaterte: Skrift: Ikke Fet

formaterte: Skrift: Ikke Fet

formaterte: Skrift: Ikke Fet

formaterte: Skrift: Ikke Fet

formaterte: Skrift: Ikke Fet

formaterte: Skrift: Ikke Fet

formaterte: Skrift: Ikke Fet

263

264

265

266

267

268

269

270

271

272

[As a first quality check we used Table 6 in McSweeney et al. \(2015\) to see if the five GCMs perform satisfactorily in the representation of two out of the three physical phenomena consisting of i\) annual temperature and precipitation cycles, ii\) circulation and iii\) storm tracks. This criterion did not lead to any exclusion of the 17 model combinations. As a next check we verify if the GCM-RCM combinations are ranked in the ‘best half’ for 24 variables and impact-based indices \(Table 2 in Vautard et al., 2021\) for the region of Scandinavia \(Figure 12a in Vautard et al., 2021\). This made us exclude cnrm_rliilpl_alaro. Further, we excluded three simulations performed with the RCM RACMO22E which are affected by a bug in the snow albedo which again strongly affects the temperature signal above and around glaciers. This bug is documented in the EURO-CORDEX Errata table. Lastly, we checked the GCM-RCMs’ performance with respect to the observed temperature](#)

and precipitation climate in Norway by using the seNorge v20.05 dataset as reference data. The largest precipitation biases (> 14 %) were found for the historical simulations with hadgem2_r1i1p1_hirham, mpi-r1i1p1_remo and ecearth-r12i1p1_remo, hence we excluded these simulations.

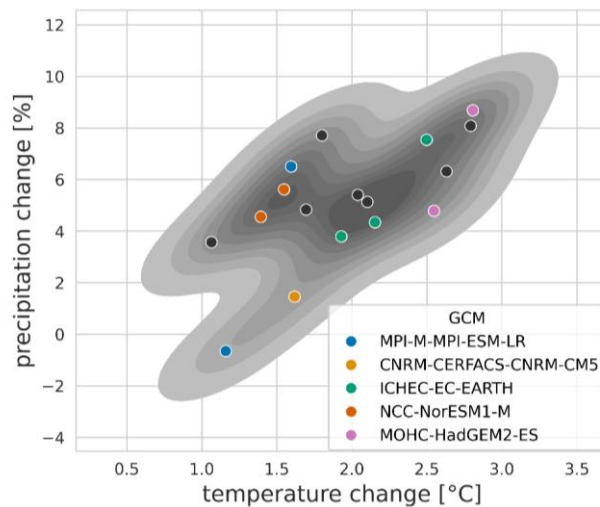


Figure 3. Projected changes in temperature and precipitation for mainland Norway by the end of the century relative to the reference period (1991–2020) century (2071–2100 minus 1991–2020) under the RCP4.5 scenario (all dots). The grey shaded area indicates the distribution (kernel density estimate) of the projected changes comprising all 17 GCM-RCM combinations that were considered. The individual coloured points highlight the ten simulations selected for CiN-2025 (Table 1).

Given time and computational constraints, we defined an upper limit of ten model combinations that are used as forcing data for the hydrological models. The ten GCMs-RCMs combinations were chosen based on the five following criteria:

- 1) High resolution (0.11 x 0.11°) simulations based on the representative concentration pathways RCP2.6, RCP4.5 and RCP8.5 are available on the Earth System Grid Federation (ESGF).
- 2) Important physical phenomena in the GCMs such as temperature and precipitation cycles, circulation and storm tracks over Europe are represented in an acceptable manner, i.e. the chosen GCM scores satisfactory for at least two of the physical phenomena (Table 6 in McSweeney et al., 2015).
- 3) Include as many plausible GCMs as possible that fulfil criteria 2 in order to capture the potential impact of the projected climate change signal.

290 ~~4) The GCM-RCM combination should be ranked in the ‘best half’ for 24 variables and impact-based indices (Table 2~~
291 ~~in Vautard et al., 2020) for the region of Scandinavia (Figure 12a in Vautard et al., 2020).~~

292 ~~5) The temperature and precipitation biases for Norway, i.e. simulated vs. observed values from seNorge2018 v20.05~~
293 ~~from 1971–2000 should not be visually striking compared to the biases in all available model combinations.~~

294 This leaves us with ~~ten~~ selected model combinations based on these five criteria are presented in Table 1. The projected
295 changes in temperature and precipitation are shown for each model combination in Fig. 3. ~~In total, these model combinations~~
296 ~~consist of five GCMs and six RCMs.~~ Based on the selection of the ten GCM-RCM combinations (coloured dots in Fig. 3),
297 the projected changes in temperature and precipitation in Norway range from 1.45–2 °C to 2.8 °C and from -1 % to 9 % in the
298 future period 2071–2100 relative to the reference period 1991–2020.

299 The selected GCM-RCM combinations vary in data coverage and quality (Table 1). The GCM ~~MOHC~~-HadGEM2-ES lacks
300 13 months towards the end of the time series, so we only used the simulations forced by this GCM until the end of 2098. When
301 looking at near (2041–2070) and far future (2071–2100) changes, the ~~MOHC~~-HadGEM2-ES simulations were shifted by two
302 years, i.e. the periods for ~~MOHC~~-HadGEM2-ES were 2039–2068 and 2069–2098. In addition, ~~MOHC~~-HadGEM2-ES driven
303 ~~EURO-CORDEX CMIP5 simulations use the HadGEM2-ES calendar with simulates~~ 360 days instead of 365 (366) days. To
304 fill in the missing five days, we simply copied the day number 150, 210, 240, 300 and 360 from the 360-day year and added
305 these extra days to the day number 151, 212, 243, 304 and 365 in a normal year. For a leap year, a copy of day number 59 was
306 added similarly. This simple technique was also used on ~~NCC~~-NorESM1-M coupled with ~~SMHI~~-RCA4 as this model
307 combination does not support leap years. Unrealistically large snow accumulation at isolated grid cells have been discovered
308 in the simulations from ~~SMHI~~-RCA4 and ~~DMI~~-HIRHAM5. They were considered as minor quality issues and their effects
309 were reduced by applying a spatial smoothing on the variables minimum, mean and maximum temperature, and humidity, an
310 approach adopted from CH2018 (2018).

311 ~~The selection criteria for the EURO-CORDEX CMIP6 projections are different from the ones for the EURO-CORDEX CMIP5~~
312 ~~projections, because there were (only) 14 RCM simulations based on CMIP6 available by June 2024 (Table S1 in~~
313 ~~Supplementary material). Also, a selection of CMIP6 GCMs providing a satisfactory performance over Europe and covering~~
314 ~~a reasonable part of the climate change signal had already been carried out for the EURO-CORDEX CMIP6 simulations by~~
315 ~~Sobolowski et al. (2025). The main criteria for the selection here were thus to include as many GCMs as possible, a balanced~~
316 ~~RCM selection and excluding model combinations that show fairly similar results in temperature and precipitation over~~
317 ~~Norway. This led us to exclude the model combinations eearthveg r1ilp1fl icon, eearthveg r1ilp1fl racmo and~~
318 ~~miroc_r1ilp1fl_hclim. We further excluded noresm_r1ilp1fl_racmo due to a low climate sensitivity and small precipitation~~
319 ~~changes during the summer months.~~

Formater: Mellomrom Etter: Automatisk

321 **Table 1. Summary of GCM-RCM combinations for RCPs which were selected for downscaling and bias adjustment for the mainland**
 322 **of Norway.**¹: Original data has 360 days only. Additional days added. ²: Leap year days added. ³: Spatial smoothing applied to
 323 **tasmin, tasmax, tas and hurs**

Model combination name	GCM model id (CMIP5)	RCM model id (CORDEX)	Data coverage
enrm-r1i1p1-aladin	CNRM-CERFACS-CNRM-CM5	CNRM-ALADIN63	1960–2100
ecearth-r12i1p1-rea ³	ICHEC-EC-EARTH	SMHI-RCA4	1970–2100
ecearth-r12i1p1-celm	ICHEC-EC-EARTH	CLMcom-CCLM4-8-17	1960–2100
ecearth-r3i1p1-hirham	ICHEC-EC-EARTH	DMI-HIRHAM5	1960–2100
hadgem-r1i1p1-rea ^{1,3}	MOHC-HadGEM2-ES	SMHI-RCA4	1970–2098
hadgem-r1i1p1-remo ⁴	MOHC-HadGEM2-ES	GERICS-REMO2015	1960–2098
mpi-r1i1p1-celm	MPI-M-MPI-ESM-LR	CLMcom-BTU-CCLM4-8-17	1960–2100
mpi-r2i1p1-remo	MPI-M-MPI-ESM-LR	MPI-CSC-REMO2009	1960–2100
noresm-r1i1p1-rea ^{2,3}	NCC-NorESM1-M	SMHI-RCA4	1970–2100
noresm-r1i1p1-remo	NCC-NorESM1-M	GERICS-REMO2015	1960–2100

324 5 Downscaling and bias-adjustment methods

325 For CiN-2015, only daily mean temperature and precipitation were bias-adjusted, but for CiN-2025, nine surface variables
 326 from the RCM outputs were downscaled and bias-adjusted, namely mean, minimum and maximum air temperature at two
 327 meters height, precipitation, mean wind speed at 10 meters height, long- and shortwave radiation, surface pressure, and relative
 328 humidity at two meters height.

329 The nine climate variables from the RCM outputs were firstly re-gridded to the seNorge grid with a 1 km spatial resolution
 330 using the nearest-neighbour method. This conservative way to downscale from a coarse to fine scale grid ensures that the
 331 original model outputs are preserved and not altered unintentionally by the downscaling step. The bias-adjustment procedure
 332 was then implemented on the grid cell basis. Depending on the variable adjusted, different reference datasets (see Section 2.2)

333 were used for calibration training. Wet-day correction has also been applied prior to bias adjustment of precipitation because
334 RCMs generally provide more rainy days than the observed ones (Frei et al., 2003).

335 Since the grid cells are bias-adjusted individually, we need to select methods that are computational efficient, or at least
336 applicable, and numerically stable (François et al., 2020) for a large number of grid cells (354 448 in total). We have tested a
337 few bias-adjustment techniques categorized as quantile mapping (Cannon et al., 2015) and multivariate approaches (François
338 et al., 2020). In the end, the univariate bias-adjustment adopting de-trended empirical quantile mapping (EQM) approach
339 (Bürger et al., 2013Gudmundsson et al., 2012) was used to bias-adjust one climate variable at a time because the method meets
340 all the aforementioned criteria and is widely used in adjusting climate model data. EQM is effective in removing the model
341 biases, preserving the trend and climate change signal moments (i.e. mean and standard deviation) and estimating extremes.
342 As no univariate method can correct the possible biases in correlation among the atmospheric variables, all the EQM results
343 were further post-processed with the multivariate 3DBC approach (Mehrota and Sharma, 2019) to rectify inter-variable,
344 temporal and spatial dependency structures.

345 5.1 EQM

346 The quantile mapping approaches establish a statistical transfer function for a variable between RCM outputs and observations
347 in the calibration period 1985–2014, which is assumed to be valid for use in the projection period. Specifically, for EQM, 12
348 calendar month-specific transfer functions were derived by fitting the empirical cumulative distribution functions (eCDFs) of
349 the modelled values with the eCDFs based on observations for each grid cell. Daily data within a 3-month window centred on
350 the month of interest were pooled and used to develop monthly eCDF to avoid overfitting (Cannon et al., 2015). For example,
351 data from February to April were used to develop the eCDF for March. The transfer function was approximated by a series of
352 empirical quantiles with fixed intervals of 0.01 spanning the probability space (0,1) (Gudmundsson et al., 2012). Only the 1st
353 to 99th quantiles were obtained and used. Linear interpolation was applied for values in between those fixed quantiles. For
354 values smaller than the 1st quantile and larger than the 99th quantile, constant linear extrapolation based on the 1st and 99th
355 quantiles was performed accordingly.

356 The projection period starting from 2015 to 2100 was further divided into seven overlapping 30-year time slices. The first time
357 slice, however, only covers 2015–2040, followed by 2021–2050, 2031–2060, etc. After the bias adjustment of each time slice
358 using the established transfer functions on a monthly basis, only the 10-year results in the middle of the period were being
359 kept. For the first and the last time slices, the results of the first 16 years and the last 20 years were used respectively. A
360 continuous time series covering the whole projection period was put together afterwards.

361 To reduce the potential impact of over-adjustment (modifying the long-term linear trend) and extrapolation (model-projected
362 values lying outside the range of the historical distribution), the long-term mean of the projected period was first removed from

363 model-projected values. This shifting of the future distribution can better secure the applicability of the transfer function based
364 on historical distribution. The long-term mean was later reimposed after the bias-adjustment of the 'residuals'. For all the
365 variables other than temperatures, long-term mean removal and reimposition were performed multiplicatively (see Cannon et
366 al., 2015, for more details). Similar linear trend removal and reimposition for the projected values of temperature variables
367 were done additively.

368 The EQM approach adopted in this study is a de-trended variant of quantile mapping method which first establishes a statistical
369 transfer function for a variable between RCM outputs and reference data in the training period 1985–2014. Twelve calendar-
370 month-specific transfer functions were derived by fitting the empirical cumulative distribution functions (eCDFs) of the
371 modelled values with the eCDFs based on reference data for each grid cell. With these monthly bias-adjustments we correct
372 model biases which are varying throughout the year. This is essential for instance to produce realistic seasonal flow patterns
373 and hydrological regimes in the subsequent hydrological modelling. To avoid overfitting, daily data within a 3-month window
374 centred on the month of interest were pooled and used to develop the monthly eCDFs (Cannon et al., 2015). For example, data
375 from February to April were used to develop the eCDF for March.

376 The transfer functions were approximated by a series of empirical quantiles with fixed intervals of 0.01 spanning the probability
377 space (0,1) (Gudmundsson et al., 2012). Only the 1st to 99th quantiles were obtained and used. Linear interpolation was applied
378 for values in between those fixed quantiles. For values smaller than the 1st quantile and larger than the 99th quantile, linear
379 extrapolation was performed based on the slopes derived from the 1st and 2nd quantiles and 98th and 99th quantiles
380 respectively. These functions are assumed to be applicable to the projection period.

381 Wet-day correction has also been applied prior to bias-adjustment of precipitation because RCMs generally provide more rainy
382 days than the observed ones (Frei et al., 2003). For each grid cell, a threshold value is derived such that the wet-day frequency
383 in modelled precipitation is equal to that in the corresponding reference data for the training period. All modelled precipitation
384 values which are below the derived threshold value are then set to zero for both training and projection periods (Gudmundsson
385 et al., 2012).

386 To reduce the potential impact of over-adjustment (modifying the long-term linear trend) and extrapolation (model-projected
387 values lying outside the range of the historical distribution), the long-term linear trend (usually 30-year) of the projected period
388 was first removed from model projections. This shifting of the future distribution can better secure the applicability of the
389 transfer function based on historical distribution. And the daily variability about the monthly mean remained unchanged. The
390 trend was later reimposed after the bias-adjustment of the 'residuals'. For all the variables other than temperatures, trend
391 removal and reimposition were performed multiplicatively. For example, relative trend for precipitation for month i , $\delta P_{i,t}$, is
392 defined as:

$$\delta P_{i,t} = \overline{P_{i,t}^{prj}} / \overline{P_{i,t}^{eng}} \quad (1)$$

formaterte: Skrift: (Standard) +Overskrifter (Times New Roman), 10 pkt

formaterte: Skrift: (Standard) +Overskrifter (Times New Roman), 10 pkt

formaterte: Skrift: (Standard) +Overskrifter (Times New Roman), 10 pkt

formaterte: Skrift: (Standard) +Overskrifter (Times New Roman), 10 pkt

formaterte: Skrift: (Standard) +Overskrifter (Times New Roman), 10 pkt

formaterte: Skrift: (Standard) +Overskrifter (Times New Roman), 10 pkt

formaterte: Skrift: (Standard) +Overskrifter (Times New Roman), 10 pkt

formaterte: Skrift: (Standard) +Overskrifter (Times New Roman), 10 pkt

formaterte: Skrift: 10 pkt

formaterte: Skrift: 10 pkt, (Intl) Cambria Math

formaterte: Skrift: 10 pkt, (Intl) Cambria Math

formaterte: Skrift: (Standard) +Overskrifter (Times New Roman), 10 pkt

formaterte: Skrift: 10 pkt

formaterte: Skrift: 10 pkt

formaterte: Skrift: 10 pkt

formaterte: Skrift: 10 pkt

formaterte: Skrift: 10 pkt

formaterte: Skrift: 10 pkt

formaterte: Skrift: 10 pkt

formaterte: Skrift: 10 pkt

formaterte: Skrift: 10 pkt

formaterte: Skrift: (Standard) +Overskrifter (Times New Roman), 10 pkt

418 5.2 3DBC

419 The bias-adjusted climate projections ~~based on~~obtained from the univariate EQM approach ~~show the same dependency~~
420 ~~structures as the uncorrected RCM simulations. were further processed with an additional step +T~~o impose inter-variable,
421 temporal and spatial dependency structures ~~obtained from the reference datasets, an additional post-processing step has been~~
422 ~~applied~~. The multivariate method we used ~~for this~~ is called 3DBC (three-dimensional bias-correction) as it adjusts along the
423 three dimensions: variables, time and space. It is described in detail in Mehrotra and Sharma (2019). 3DBC is re-establishing
424 the spatial, temporal and inter-variable structures from the reference data by reordering the daily EQM values according to
425 observed time-ranks at each grid-point, resulting in the bias-adjusted data having the same rank structure (ordering) as the
426 reference data in the calibration period. Compared to other multivariate bias correction methods (e.g. the MBCn method
427 developed by Cannon, 2018) the computational requirements of 3DBC are relatively small, making its application on a large
428 number of grid cells feasible. Note that 3DBC adjusts the ranks for future periods according to changes in the ~~variable-temporal~~
429 auto-correlations as simulated by the RCMs. Thus, it does not strictly assume that the dependency structures remain stable in
430 future climates. However, while the original implementation by Mehrotra and Sharma (2019) works on single calendar days
431 across a future period of 30 years, our future period (2021-2100) consists of 80 years. Following the original approach would
432 have resulted in imposing observed trends repeatedly on the future period. We thus adapted the 3DBC method to work within
433 single years of the EQM data, an ~~ansatz approach~~ that maintains the climate change signals ~~and trends~~ from the RCMs (and
434 EQM) on an annual scale. As a result, the adjustments in the variable auto-correlations for the future periods have a limited
435 effect and do not fully transfer the dependency structure changes from the RCMs to the 3DBC bias-adjusted data. ~~Since 3DBC~~
436 ~~reshuffles the bias-adjusted times series resulting from EQM within a year, the marginal distributions at seasonal scale might~~
437 ~~be modified~~.

438 5.3 Evaluation of bias-adjustment methods

439 5.3.1 Performance of bias-adjustment methods

440 Thorarinsdottir et al. (2013) proposed the use of integrated quadratic distance (IQD) as a performance measure to compare the
441 full distribution of climate model output to the corresponding distribution of observed data. IQD was further employed by
442 Yuan et al. (2019; 2021) to assess the performance of different bias-adjustment approaches. IQD (Eq. 64) is defined as:

$$443 d_{IQ}(F, G) = \int_{-\infty}^{+\infty} (F(t) - G(t))^2 dt \quad (64)$$

444 where F, G are two cumulative distribution functions. $d_{IQ}(F, G)$ summarizes the differences, and a lower value implies a
445 smaller difference between F and G . $d_{IQ}(F, G) = 0$ if $F = G$. For further details, please see Thorarinsdottir et al. (2013). In this
446 study, we compared the eCDFs of bias-adjusted precipitation and temperature with corresponding seNorge2018 v20.05 data
447 over the ~~calibration-training~~ (1985–2014) and validation (1960–1984 or 1970–1984 depending on the period start of the

448 RCM) periods in each grid cell. In addition, we calculated IQD scores derived from comparison of original RCM outputs with
 449 the observed data.

450 IQD scores for precipitation and temperature are presented in Table 2 Fig. 4, are averaged over all grid cells and GCM-RCM
 451 combinations. We evaluated and ranked the bias-adjustment methods according to the IQD scores averaged on an annual and
 452 seasonal basis. The results clearly demonstrate that both bias-adjustment approaches are far better at reproducing the full
 453 distributions of observed precipitation and temperature by several orders of magnitude than the original RCM outputs. As
 454 expected, the improvements are larger (smaller d_{IQ}) in the calibration-training period than the validation period. EQM and
 455 3DBC have the same performance on annual results, but Furthermore, 3DBC generally performs better overall than EQM on
 456 seasonal results because 3DBC utilizes additional information about the intra-annual order of the observed time series in the
 457 post-processing, whereas the annual results remain the same. The only exceptions are the IQD scores from particular RCMs
 458 (CCLM4-8-17, REMO2015 and REMO2009), which show that EQM provides marginally better results than 3DBC in autumn
 459 (Fig. S1 in Supplementary materials). It might indicate that the observed ranks in autumn of the training and validation periods
 460 are quite different and that those models capture this change. Thus Overall, 3DBC provides added value as compared to
 461 EQM when seasonal statistical properties are of importance.

462 Table 2: Integrated quadratic distance (IQD) scores comparing cDFs derived from two bias-adjustment approaches (EQM and
 463 3DBC) in addition to original RCM outputs with reference datasets seNorge2018 v20.05 over the calibration (1985–2014) and
 464 validation (1960/70–1984) periods. All IQD scores are averages over all grid cells and GCM-RCM combinations. The best
 465 performance on each time scale is indicated in bold italic.

	Calibration			Validation		
	Original	EQM	3DBC	Original	EQM	3DBC
Precipitation						
Annual	1.17E-01	2.27E-05	2.27E-05	1.32E-01	7.19E-03	7.19E-03
Winter (DJF)	1.61E-01	1.65E-03	5.61E-04	1.87E-01	2.90E-02	8.42E-03

Spring (MAM)	1.16E-01	6.42E-04	<i>2.50E-04</i>	1.52E-01	2.04E-02	<i>5.22E-03</i>
Summer (JJA)	1.34E-01	1.21E-03	<i>3.50E-04</i>	1.47E-01	1.11E-02	<i>8.09E-03</i>
Autumn (SON)	1.60E-01	1.03E-03	<i>3.79E-04</i>	1.42E-01	1.37E-02	<i>1.04E-02</i>
Temperature						
Annual	1.81E-01	<i>9.98E-05</i>	<i>9.98E-05</i>	1.91E-01	<i>1.37E-02</i>	<i>1.37E-02</i>
Winter (DJF)	3.59E-01	1.71E-03	<i>1.40E-03</i>	4.26E-01	7.73E-02	<i>5.21E-02</i>
Spring (MAM)	3.00E-01	3.40E-03	<i>1.06E-03</i>	2.97E-01	2.77E-02	<i>1.84E-02</i>
Summer (JJA)	5.72E-01	1.59E-03	<i>7.09E-04</i>	6.38E-01	3.03E-02	<i>2.41E-02</i>
Autumn (SON)	1.79E-01	1.69E-03	<i>9.86E-04</i>	1.82E-01	1.81E-02	<i>1.45E-02</i>

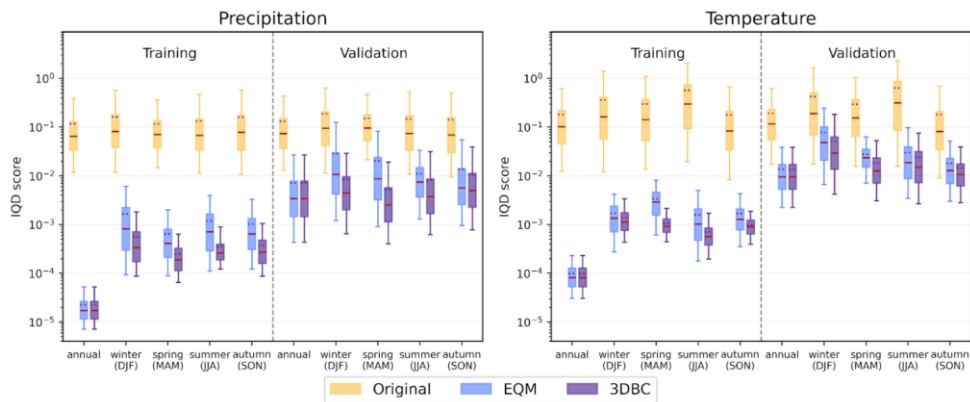
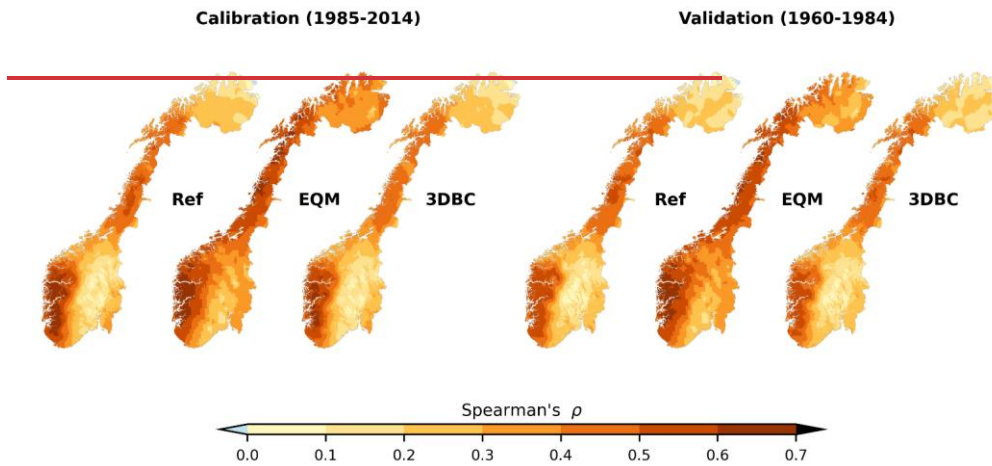


Figure 4: Integrated quadratic distance (IQD) scores for precipitation (left panel) and temperature (right panel) based on the CMIP5 model ensemble. Bias-adjusted results from EQM and 3DBC in addition to the original model outputs are compared with the reference datasets seNorge2018 v20.05 over the training (1985–2014) and validation (1960/70–1984) periods. The red line on the box indicates the median value whilst the dotted line represents the mean. The lower and upper boundaries of the box are the 25th and 75th percentiles. The lower and upper ends of the whiskers refer to the 5th and 95th percentiles.

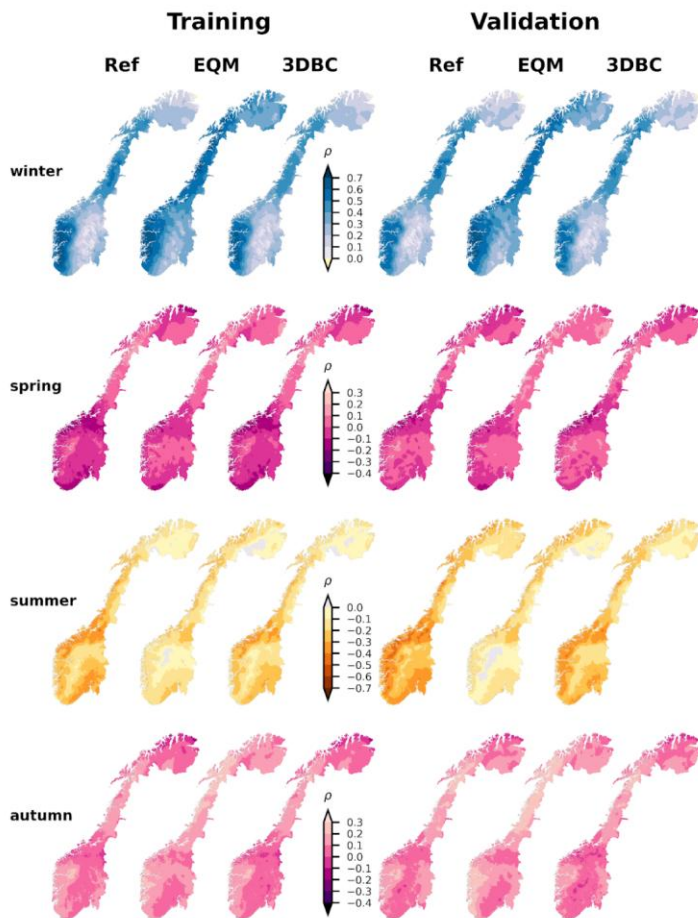
formaterte: Engelsk (USA)

Besides the seasonal statistics, 3DBC can simulate better spatial correlation structures between precipitation and temperature in the historical period than EQM, as 3DBC as a post-processing procedure follows the ranks of observed precipitation and temperature. It reorders the modelled ranks of precipitation and temperature based on observations while the univariate EQM method keeps the spatial rank correlation pattern from the RCM results accordingly and can simulate the spatial correlation structures between these two variables in the historical period better than EQM can achieve. Figure 5 shows an example of the spatial distribution of seasonal Spearman's rank correlation coefficient (ρ), calculated based on the bias-adjusted datasets from EQM and 3DBC and the reference datasets for training (1985–2014) and validation (1960–1984) periods for one RCM. In general, ρ are largest and positive in winter (warm days are wetter), followed by negative ρ in summer (warm days are dry, cold are wet). In spring and autumn, ρ is much smaller than in summer and winter, indicating a rather weak rank correlation between precipitation and temperature. The differences in the spatial correlation structure between these two methods are often most pronounced in winter and summer. EQM usually overestimates the positive rank correlations almost over the whole country in winter, whilst it underestimates negative dependencies in summer. And this spatial rank correlation pattern seems to be rather stable from one period to another. Aggregated results for each model combination are shown as boxplots (Fig. S2

486 in Supplementary materials), and they confirm that 3DBC performs better in recovering the inter-variable spatial dependency
487 structure for all RCMs. EQM inherits the spatial rank correlation pattern from the RCM. The seasonal differences between
488 these two methods are often most pronounced in winter (DJF) and summer (JJA). Figure 4 shows an example for winter,
489 comparing the bias-adjusted datasets from EQM and 3DBC with the reference datasets for calibration (1985–2014) and
490 validation (1960–1984) periods for one RCM. EQM generally overestimates the rank correlations between precipitation and
491 temperature almost over the whole country in winter. And this spatial rank correlation pattern seems to be rather stable from
492 one period to another. Generally, the results confirm that 3DBC performs better in recovering the inter-variable spatial
493 dependency structure.



494

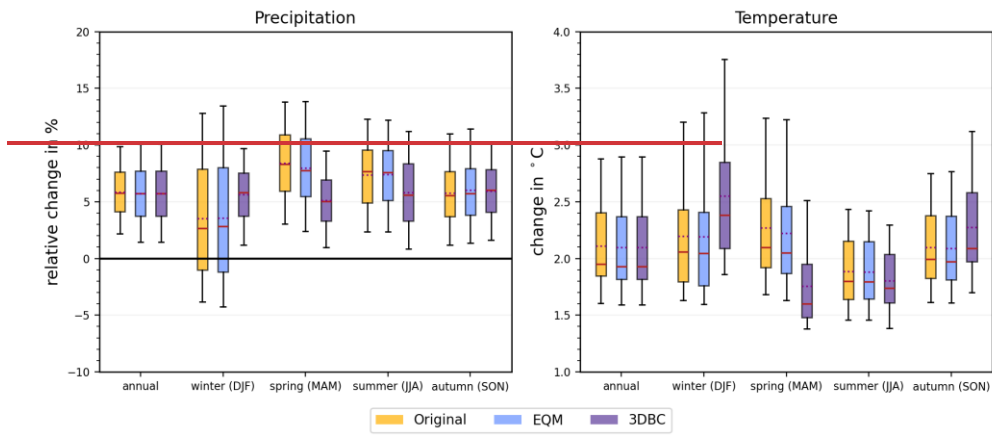


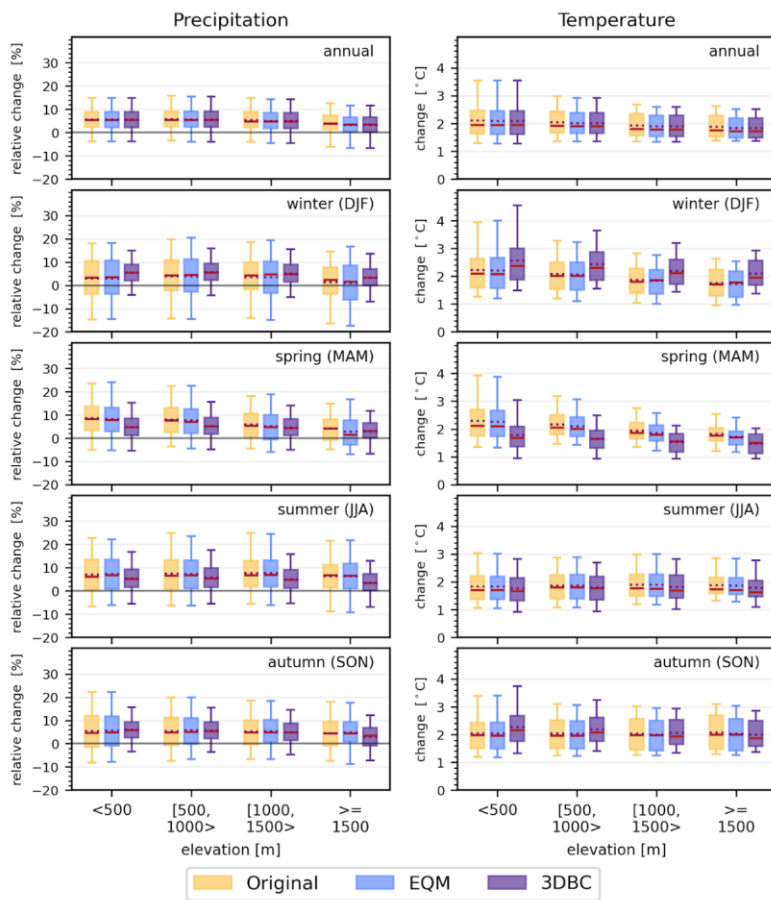
495
496
497
498
499

Figure 54: Spatial distribution of Spearman's r-Rank correlation coefficient ρ of daily precipitation and temperature in winter (DJF), spring (MAM), summer (JJA) and autumn (SON) for the two bias-adjustment methods. For calibration-training (1985–2014) and validation (1960–1984) periods, the two bias-adjusted datasets, EQM and 3DBC are based on historical run from CMIP5-based mpi-r1i1p1-cclm and compared with reference datasets seNorge2018 v20.05.

5.3.2 Climate change signal preservation

The two bias-adjustment methods can lead to different climate change signals in the future periods (e.g. 2071-2100) relative to the reference period (1991-2020). Figure 6 shows the annual and seasonal changes grouped in four elevation bands (< 500, [500, 1000>, [1000,1500>, > 1500), including 52%, 32.7%, 13.6% and 1.7% of the grid cells in Norway, respectively. The result aligns with other recent studies demonstrating that the change signals are elevation-dependent (Astagneau et al., 2025, Matiu et al., 2024). The two bias-adjustment methods provide identical annual climate change signals, since 3DBC uses the same bias-adjusted results from EQM before further post-processing. EQM generally preserves the seasonal climate change signals from the original RCMs in terms of both mean and median changes as well as the spread of changes for all elevation bands. However, by reshuffling the chronological order intra-annually, 3DBC modifies the seasonal change signals from the original RCMs, leading to larger increases in precipitation and temperature in winter and smaller increases in spring than the original RCM outputs. In summer and autumn, the climate change signals can be underestimated or overestimated by 3DBC depending on the variables and elevations. When comparing the two methods of bias adjustment in terms of climate change signals, EQM preserves the original climate change signals from the climate models better than 3DBC (Fig. 5). For precipitation, the larger increase in relative changes in winter for 3DBC than EQM are offset by smaller increases in relative changes in spring and summer. Changes in temperature show similar characteristics. Larger positive winter temperature changes for 3DBC are compensated by smaller positive spring temperature changes. The spreads of the changes are comparable between EQM and the original model outputs. 3DBC, on the other hand, exhibits varying spreads depending on the seasons and variables, as the climate change signal preservation is not strictly prescribed in the method. On an annual basis, these two methods provide identical results since 3DBC uses the same bias-adjusted results from EQM before further post-processing. By reshuffling the chronological order intra-annually, 3DBC modifies the seasonal change signals substantially.





521
 522 **Figure 6: Projected annual and seasonal changes in precipitation (relative change in %, left column) and temperature (change in**
 523 **°C, right column) from 1991–2020 to 2071–2100 for RCP4.5 in terms of elevation. Results grouped in four elevation bands from two**
 524 **bias-adjustment procedures, EQM and 3DBC, are compared to the original RCM projections. The red line on the box indicates the**
 525 **median value whilst the dotted line represents the mean. The lower and upper boundaries of the box are the 25th and 75th percentiles.**
 526 **The lower and upper ends of the whiskers refer to the 5th and 95th percentiles.** Figure 5: Comparison of projected annual and seasonal
 527 **changes in precipitation (relative change in %, left panel) and temperature (change in °C, right panel) from 1991–2020 to 2071–2100**

for RCP4.5. Results averaged over all grid cells and RCM model ensemble from two bias adjustment procedures, EQM and 3DBC, are compared to the original RCM projections. The thick red line on the box indicates the median value whilst the dotted line represents the mean. The lower and upper boundaries of the box are the 25th and 75th percentiles. The lower and upper ends of the whiskers refer to the 5th and 95th percentiles.

6 Hydrological modelling

6.1 DistHBV

DistHBV is a spatially distributed version of the HBV precipitation-runoff model (Beldring et al., 2003) and is the major tool applied to assess hydrological responses to climate change in Norway. The model calculates the water balance for 1 x 1 km grid cells at a daily time step covering the entire mainland surface area of Norway and upstream areas in Finland and Sweden contributing to streamflow in Norwegian catchments. Each grid cell includes one soil type and up to five land cover types. DistHBV has components for accumulation, sub-grid scale distribution and ablation of snow, interception storage, sub-grid scale distribution of soil moisture storage, evapotranspiration, groundwater storage and runoff response, lake evaporation and glacier mass balance. The newly implemented Penman-Monteith method and the prescribed parameterizations are presented in Huang et al. (2019) and Erlandsen et al. (2021).

As for other conceptual hydrological models, calibration is necessary to adjust the DistHBV parameters to improve the model performance of reproducing observed discharge, due to the absence of directly measured catchment characteristics, natural variability and the non-linearity of the processes involved. Since all parameters to calculate potential evaporation are prescribed in the Penman-Monteith equation, the calibration parameters are mainly associated with lake, subsurface, and snow and glacier processes (Table 2). There are ten main calibration parameters (Table 3), of which Different from the lumped version of HBV, the parameters associated with snow and subsurface processes in distHBV three are vary by land use cover type (deciduous forest, coniferous forest and others) specific and six are soil specific (the five soil types based on the sediment map (Section 2.3) plus glacier bed), respectively. In total, there are 44 parameters for modelling mainland of Norway, including six snow parameters (two snow parameters times three land use classes), 36 soil parameters (six soil types times six subsurface parameters) and two parameters associated with lake and glacier processes. The parameters vary between grid cells due to different combinations of soil and land cover types within grid cells. Note that we didn't distinguish the snow parameters for all land cover types because it will increase equifinality risks due to too many calibration parameters and forest is one of the dominant land cover types in Norway (Huang et al., 2026). In addition, we didn't calibrate the rainfall or snow correction parameters as in other HBV applications, because it will lead to inconsistency between the climate and hydrological projections in terms of water balance, resulting in a total of 44 parameters.

Table 23: list of calibration parameters. Note that the parameters in associated with the land use snow and soil subsurface categories processes vary across by land use cover and soil types, respectively.

Category	Parameter	Explanation	Unit	Min	Max
Lake	KLAKE	Rating curve constant	-	1.00E-04	0.1
	SMELT_T	Snow melt temperature	°C	-1	2
Landuse	SMELTR	Temperature index for snow melt rate	m/°C	1.00E-04	0.01
	IMELTR	Ice melt rate for glaciers additional coefficient to SMELTR	-	1	4
	FC	Field capacity	m	1.00E-02	1
	BETA	Shape coefficient of soil moisture	-	1	5
	KUZ	Upper zone recession coefficient	-	1.00E-03	1
	ALFA	Upper zone nonlinear drainage coefficient	-	1	2
	PERC	Percolation from upper zone to lower zone	-	1.00E-03	0.5
Soil	KLZ	Lower recession coefficient	-	1.00E-03	1

Associated process	Parameter	Explanation	Unit	Min	Max
Lake	KLAKE	Rating curve constant	-	1.00E-04	0.1
	SMELT_T	Snow melt temperature	°C	-1	2
Snow and glacier	SMELTR	Temperature index for snow melt rate	m/°C	1.00E-04	0.01
	IMELTR	Ice melt rate for glaciers additional coefficient to SMELTR	-	1	4
	FC	Field capacity	m	1.00E-02	1
	BETA	Shape coefficient of soil moisture	-	1	5
	KUZ	Upper zone recession coefficient	-	1.00E-03	1
	ALFA	Upper zone nonlinear drainage coefficient	-	1	2
	PERC	Percolation from upper zone to lower zone	-	1.00E-03	0.5
Subsurface	KLZ	Lower recession coefficient	-	1.00E-03	1

The model was calibrated against discharges at 85 gauges (Fig. 1) from 2000 to 2007 using the parameter estimation routine PEST (Doherty and Skahill, 2006) and a multi-criteria calibration approach (Huang et al., 2019). The multi-criteria include the Nash and Sutcliffe efficiency (NSE) (Nash and Sutcliffe, 1970), the bias in water balance (BIAS) and the volume bias in the high-flow segment of the flow duration curve (ΔFHV , 0 – 0.02 flow exceedance probabilities) (Yilmaz et al., 2008). Since PEST minimizes the difference between the criteria results and their ideal values (1 for NSE and 0 for biases), the calibration objective function θ containing the three criteria at multiple gauges can be formulated as Eq. 72.

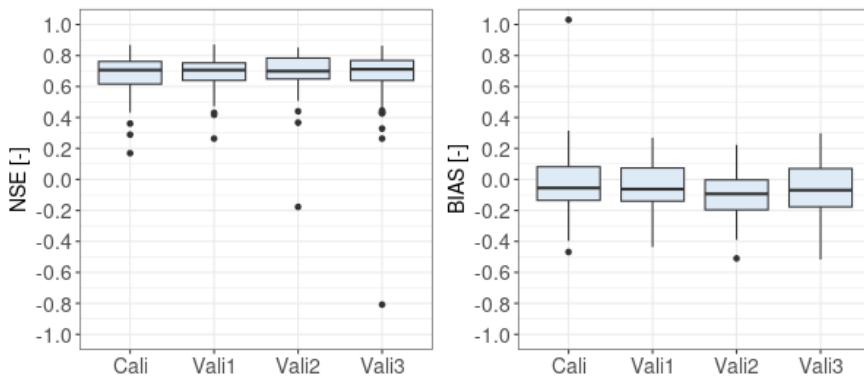
$$\theta = W_{NSE} * \sum_{i=1}^n (1 - NSE_i)^2 + W_{BIAS} * \sum_{i=1}^n (BIAS_i)^2 + W_{\Delta FHV} * \sum_{i=1}^n (\Delta FHV_i)^2 \quad (72)$$

where W are weights for each criterion and $n = 85$, the number of calibration catchments. W_{NSE} equals to 8 and W_{BIAS} and $W_{\Delta FHV}$ equal to 1 to achieve a good calibration performance.

Five PEST runs were carried out with different initial parameter values and only the parameter set giving the best model performance was selected for model validation. The model was validated against the discharge of the 85 calibration stations and additional 38 gauging stations from 2008-2011 to 2014-2020 to evaluate the temporal and spatial transferability of the

574 model, respectively. The validation period (2011 – 2020) was selected because it is the warmest period for most catchments
 575 in the recent decades. Compared to the calibration period (2000 – 2007), the average increase in annual mean temperature of
 576 all 123 catchments is about 0.43 degrees in 2011 – 2020. Hence, the validation results show the model performance under
 577 warmer conditions. Finally, long-term model performance is assessed based on the discharge of all 123 gauges from 1981 to
 578 2014.

579 Figure 6-7 shows the calibration and validation results in terms of NSE and BIAS. During the calibration period, about 50%
 580 and 29% of the catchments show good ($NSE > 0.65$ and $|BIAS| < 0.1$) and satisfactory ($0.65 > NSE > 0.55$ and $0.1 < |BIAS| < 0.15$)
 581 results (Moriassi et al., 2007), respectively. The model generally underestimates discharge with the median bias of -5%, mainly
 582 due to underestimation of precipitation in seNorge2018 v20.05 data. The model performs similarly in terms of median-NSE in
 583 the validation period for the 85 gauging stations, with the median NSE degraded by only 0.01, but underestimates the discharge
 584 for about 75% of the 38 gauges. The median bias is reduced by 0.025 in the validation period than in the calibration period but
 585 there are more catchments with $|BIAS| > 0.1$. The model performance varies with time, partly due to parameter transferability
 586 problems under different climate conditions and partly due to the quality of seNorge2018 v20.05 dataset that also varies with
 587 time (Lussana et al., 2019; 2020). The validation results for the additional 38 gauging stations show robust spatial
 588 transferability of the model, with good or satisfactory ($NSE > 0.55$ and $|BIAS| < 0.15$) model performance for about 58% of the
 589 catchments. The model generally underestimates discharge with BIAS less than -0.1 for about half of the validation gauging
 590 stations. Nevertheless, the validation results for the whole historical period (1981–2014) are similar to the calibration results
 591 in terms of both NSE and BIAS, indicating a robust long-term model performance. Such calibration and validation results are
 592 acceptable with consideration of the quality of the meteorological forcing data in such a mountainous region and simultaneous
 593 calibration for all catchments.



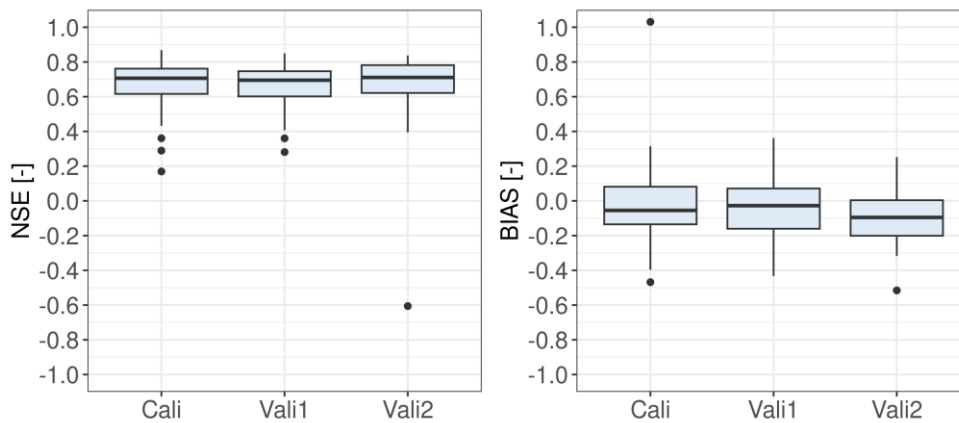


Figure 76: DistHBVdistHBV model performance in terms of NSE and BIAS for the 85 calibration catchments in the calibration period 2000 – 2007 (Cali), for the 85 calibration catchments in the validation period 2008-2011 – 2014-2020 (Vali1) and, for the 38 validation catchments in the validation period 2008-2011 – 2014-2020 (Vali2) and for all 123 catchments in the period 1981-2014 (Vali3).

6.2 DEW

Distributed Element Water balance model (DEW) hydrological model (Beldring, 2008; Li et al., 2015) was used to calculate simulate climate change impacts on glaciers and hydrological processes for 12 given glacier regions in Norway. The smallest glaciers (< 1 km²) were omitted in the DEW model. This model differs from DistHBV in the respect that it also calculates changes in glacier ice area, volume and surface elevation, and water balance. In addition, the model requires additional information as input, such as ice thickness and glacier area for grid cells with glaciers. Although However, the glacier module in DEW is more advanced than in DistHBVdistHBV, DEW uses only daily mean temperature and precipitation as meteorological forcing data as it uses a temperature-based degree-day model to estimate potential evapotranspiration, and it uses only daily mean temperature and precipitation as forcing data. Snow and glacier ice melt were calculated using a degree-day model, with different degree-day factors for snow and ice.

Snow and glacier ice melt were calculated using a degree-day model, with different degree-day factors for snow and ice. DEW applies a simplified model called DeltaH (Huss et al., 2010) to describe the changes in glacier ice area, volume and surface elevation. The method simulates the impacts of ice movement that transports mass from the highest to the lowest areas of the

614 glacier. Simulations without taking this redistribution of glacier ice into account will give incorrect estimates for both glacier
615 changes and the water flow from the glacier. It is based on historically observed elevation changes of the glacier surface
616 elevation and how these are distributed over the glacier area. The pattern of change is then used when simulating the
617 development of glacier ice area, volume and surface elevation under climate scenarios by having the model redistribute mass
618 over the glacier at the end of each mass balance year. Ice melt caused by negative mass balance results in diminishing of the
619 glacier ablation area. Simulations with more advanced, physically based glacier models that simulate the flow of ice in the
620 glaciers would probably be more realistic but are more demanding to run and require much more input data than are not
621 available for most glacier areas in Norway.

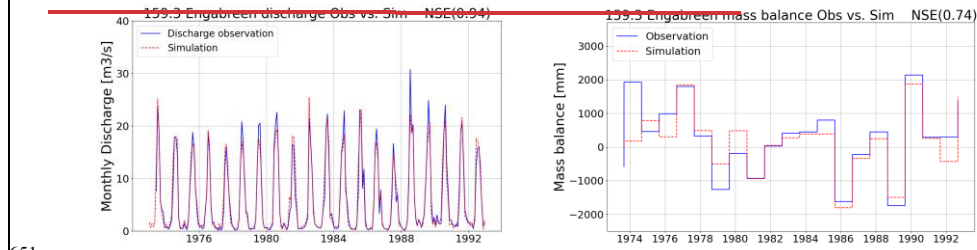
622 ~~DEW was calibrated using the same parameter estimation routine (PEST) as used for distHBV. Different from the~~
623 ~~DistHBVdistHBV-model, but it~~DEW was calibrated against observed daily streamflow and annual mass balance data for six
624 out of the ~~twelve-12~~ glacier regions. Within each of the six regions, one optimal model parameter set was determined for all
625 glaciers and catchments. This strategy was chosen to avoid discontinuities in model results between or along catchment
626 boundaries and ice divides. ~~For the remaining six glacier regions where there were no streamflow data available, model~~
627 ~~parameters were transferred from the nearest glacier region with calibrated parameters.~~ Fixed periods were not used for
628 calibration and validation as in the case of ~~DistHBVdistHBV~~, because the availability of observed data varied both in time and
629 space. It was a challenge to find both mass balance and streamflow time series of good quality at the same period, leading to
630 limited time series available for model validation in some cases. ~~DEW was calibrated using the same parameter estimation~~
631 ~~routine (PEST) as used for distHBV.~~ During model calibration, mean NSE value is 0.75 for daily discharge of 19 gauging
632 stations downstream of the glaciers, and 0.72 for annual mass balance for six glaciers. The mean NSE value for daily discharge
633 during model validation is 0.74. ~~For the remaining six glacier regions where there were no streamflow data available, model~~
634 ~~parameters were transferred from the nearest glacier region with calibrated parameters.~~

635 Although the glacier module in DEW is more advanced than in ~~DistHBVdistHBV~~, DEW uses a temperature-based degree-day
636 model to estimate potential evapotranspiration, and it uses only daily mean temperature and precipitation as forcing data. Snow
637 and glacier ice melt were calculated using a degree-day model, with different degree-day factors for snow and ice.

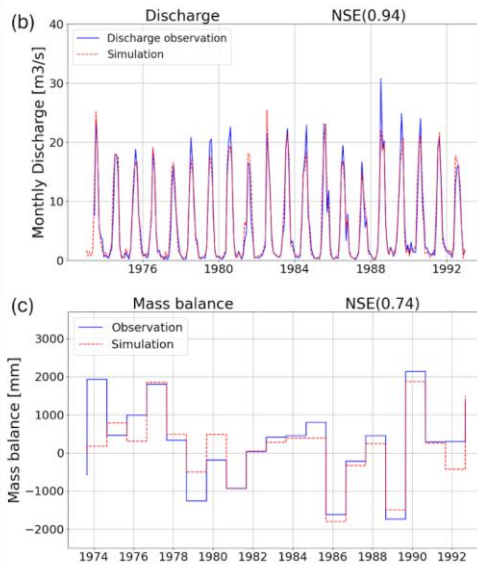
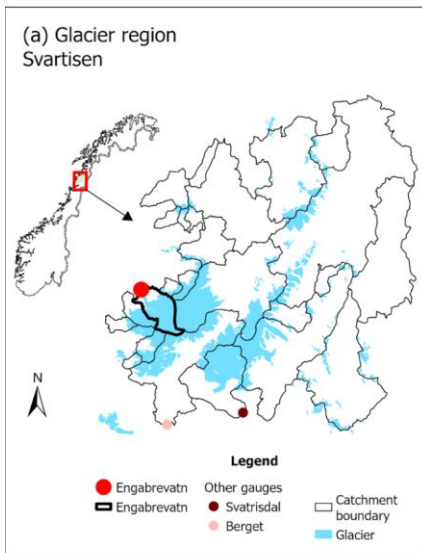
638 ~~DEW was calibrated using the same parameter estimation routine (PEST) as used for distHBV.~~ During model calibration,
639 mean NSE value is 0.75 for daily discharge of 19 gauging stations downstream of the glaciers, and 0.72 for annual mass
640 balance for six glaciers. The mean NSE value for daily discharge during model validation is 0.74.

641 ~~Figure 8a shows one of the 12 glacier regions, called Svartisen, as an example. Figure 7~~For this region, DEW was setup for
642 ~~all catchments where glacier melt contributes to river discharge. Among these catchments, only three catchments (Engabrevatn,~~
643 ~~Svartisdal and Berget) have discharge observations in good quality and only Engabrevatn has the measured mass balance data.~~
644 ~~Based on the data availability of both discharge and mass balance data, DEW was calibrated against the discharge of the three~~

645 catchments and glacier mass balance in Engabrevatn for the period 1974–1993. The calibrated parameters were then
 646 transferred to other catchments of this region for hydrological projections. Figure 8b and 8c compare the observed and
 647 simulated discharge and mass balance for Engabrevatn in the calibration period. It shows that the model can well reproduce
 648 both monthly discharge and annual glacier mass balance with NSE larger than 0.7. compares the observed and simulated
 649 discharge and mass balance for one of the best performing glacierized catchment (Engabreen) as an example. It shows that the
 650 model can well reproduce both monthly discharge and annual glacier mass balance with NSE larger than 0.7.



651

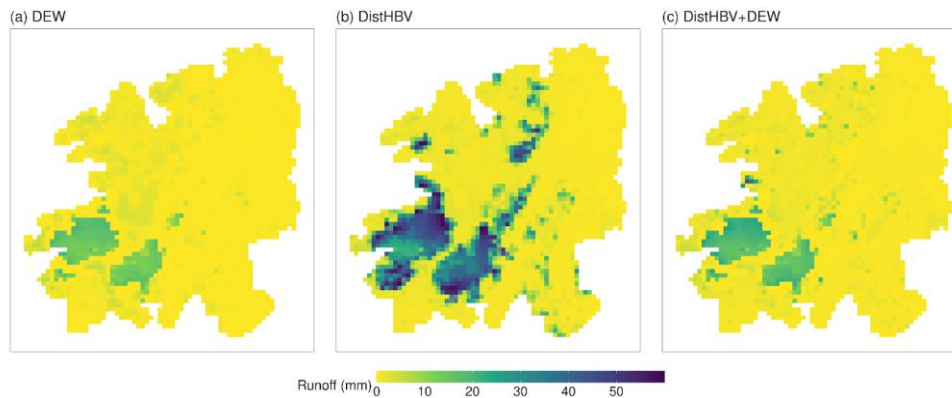


652

653 **Figure 87: The glacier region Svartisen (a), observed and simulated discharge (left) and annual mass balance (right) for the**
654 **catchment Engabrevatnen.**

655 **6.3 Postprocessing of distHBV and DEW outputs**

656 The final runoff projections for mainland Norway were produced by replacing distHBV outputs with the DEW ones. Note that
657 DEW simulated the whole glacierized catchments (Fig. 8a) but only the outputs for the grid cells with glaciers were used to
658 replace the distHBV results. It is mainly because DEW uses a simpler potential evapotranspiration (PET) method and rougher
659 landuse/soil classes than distHBV. Figure 9 (a and b) shows the simulated runoff projections using DEW and distHBV for the
660 glacier region Svartisen (Fig. 8a) on 31st August 2100 driven by the ecearth-r12i1p1-cclm climate projection. Without
661 considering glacier retreat, distHBV projected high runoff (> 20 mm) for most grid cells where glaciers exist at present while
662 DEW projected much lower runoff for these grid cells than distHBV, confirming that distHBV overestimates runoff under
663 warming conditions. After we replaced the distHBV results with the DEW ones, the final output is more reasonable for this
664 region than the distHBV one (Fig. 9c). Note that there are still single grid cells with high runoff in the final product because
665 of different glacier masks used by DEW and distHBV. In addition, small glaciers outside the glacierized catchments (Fig. 8a)
666 were not simulated by the DEW model and the results for these small glaciers cannot be corrected.



668 **Figure 9: Simulated runoff on 31st August 2100 for the glacier region Svartisen by DEW (a), distHBV (b) and the combination of**
669 **distHBV and DEW (c) driven by the ecearth-r12i1p1-cclm climate projection.**

formaterte: Skrift: 9 pkt, Fet

formaterte: Skrift: 9 pkt, Fet

formaterte: Skrift: 9 pkt, Fet

formaterte: Skrift: 9 pkt, Fet

formaterte: Skrift: 9 pkt, Fet

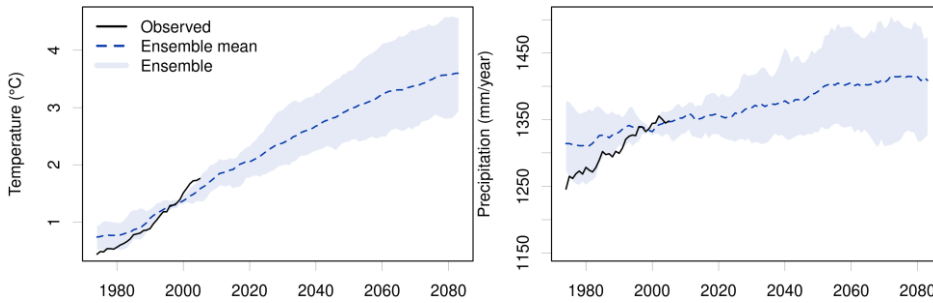
formaterte: Skrift: 9 pkt, Fet

formaterte: Skrift: 10 pkt, Ikke Fet

671 **7 National climate projections**

672 **7.1 Ensemble means and ranges**

673 There are 20 climate projections for mainland Norway at 1km spatial resolution with daily time steps under the RCP4.5
674 scenario from the COR-BA-2025 dataset. Figure 108 shows 30-year running means of annual temperature and precipitation
675 sums from 1971 to 2098 for Norway. There is a clear increase in temperatures visible in the mean and the whole ensemble.
676 For precipitation, the ensemble mean is also increasing but the lower limit of the projection ensemble is showing a stable
677 precipitation amount of about 1325 mm/year. The observed historical values are mostly within the simulated precipitation and
678 temperature ensembles but are located at the lower end of the ensemble before the year 2000 and at the upper end afterwards,
679 indicating that the RCP4.5 ensemble underestimates recent temperature and precipitation trends in Norway. Note that all RCMs
680 are bias-adjusted to match the observed values averaged over the training-period 1985-2014 and the spread in the ensemble
681 equals zero for the middle of that period (year 2000). In addition, the ensemble spread is exactly the same for both EQM and
682 3DBC methods as 3DBC has the same change statistics as EQM on an annual basis.



683
684 **Figure 108:** Simulated 30-year running means of temperature (left) and precipitation (right) from the COR-BA-2025 ensemble of
685 20 climate projections (10 GCM-RCM combinations x 2 bias-adjustment methods) for Norway under the RCP4.5 emission scenario.

686 Looking at the spatial distribution of changes from the reference period 1991–2020 to the far future period 2071–2100 (Fig.
687 119), a generally larger increase in temperatures towards the North is apparent, with about one to two °C in the southern and
688 two to three °C in the northern half of Norway. Precipitation is increasing as well with exceptions of some isolated areas along
689 the coast and in the mountains. Generally, the precipitation increases are small and below +12%.

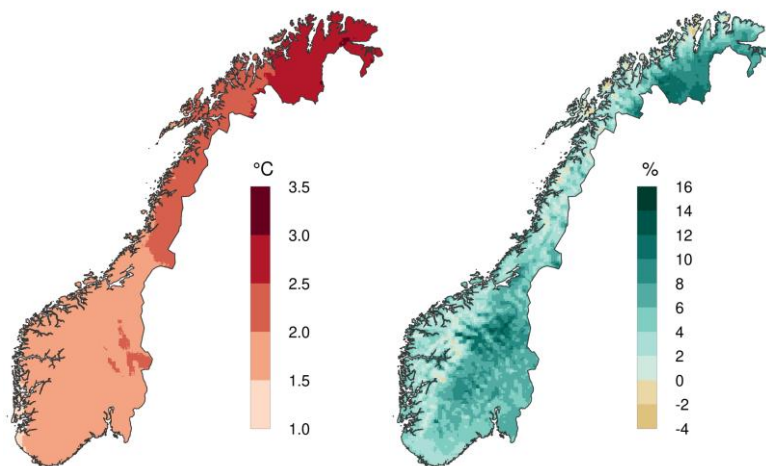
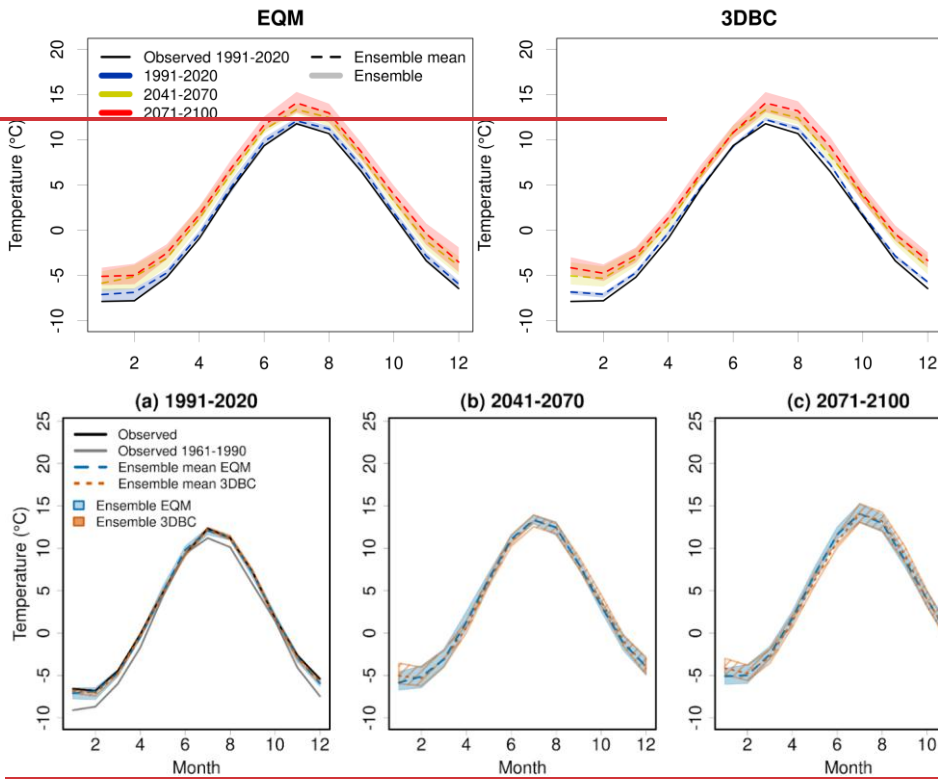


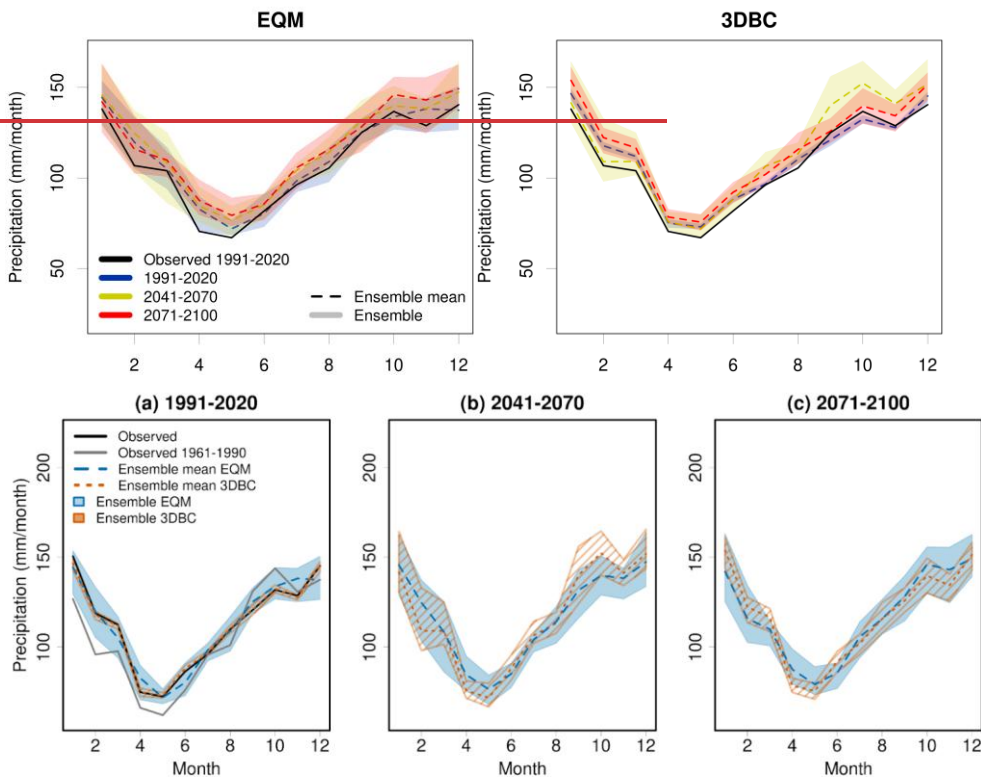
Figure 119: COR-BA-2025 ensemble mean (left) changes in temperature (°C) (left) and (right) relative changes in precipitation (%) (right) in the scenario period 2071–2100 relative to the reference period 1991–2020 under the RCP4.5 scenario for mainland Norway.

7.2 Effects of two bias-adjustment methods

The effects of the two bias-adjustment methods on the preservation and altering of the seasonal climate change signals of the RCMs is shown in Fig. 5-6 and discussed in Section 5.3.2. Similarly, the two methods have different effects on the monthly climate change signal due to their design. While EQM is designed to preserve the monthly climate change signals, the 3DBC method is designed to provide spatial, temporal and inter-variable structures based on the reference data. However, as can be seen in Fig. 4-12 and 4-13, the shapes of the climatologies from EQM and 3DBC are similar and in agreement with the observed ones. As already seen for the seasonal changes (Fig. 5-6), precipitation and temperature changes in 3DBC are larger than in EQM in winter months (especially January and February) and smaller in spring and summer (April to June) for the far future period (2071–2100). For the near future (2041–2070), the difference in the changes from EQM and 3DBC are less systematic but 3DBC shows a more-pronounced increase in autumn precipitation which is absent in the EQM (Fig. 4-13). This shift in the 3DBC results can be traced back to its implementation: the rank structure from the reference years 1961-1990 are used for the 2041-2070 period. Since the autumn precipitation in the period 1961-1990 has been large (Fig. 13a), this is imprinted on the mean annual cycle of the near future period. For the current climate (1991–2020), the 3DBC method results in climatologies that are similar for all models and thus a small ensemble-spread compared to the EQM data. This is especially true for precipitation (Fig. 4-13).



708
709
710 **Figure 4912:** 30-year mean monthly temperatures for Norway for different time periods using the EQM (left) and 3DBC (right)
711 bias-adjusted climate projections, under the RCP4.5 scenario. Black line: Observed temperature in 1991–2020. Grey line: Observed
712 temperature in 1961–1990. Blue and orange lines: ensemble means of simulated temperature. Blue and orange striped areas:
713 ensemble spread of 10 projections.



714
715
716 **Figure 131:** 30-year mean monthly precipitation amounts for Norway for different time periods using the EQM (left) and 3DBC
717 (right) bias-adjusted climate projections. The same as Fig. 12 but for precipitation.

718 7.3 Uncertainty analysis

719 Besides the two different bias-adjustment methods, the various GCM-RCM combinations contribute to uncertainties in the
720 climate projections. In this section, we analyse the contribution of these two uncertainty sources using the ANOVA method
721 used by Vetter et al. (2017). Since each GCM is combined with different RCMs (see Section 4), we don't distinguish the
722 GCMs and RCMs as different uncertainty sources here, but consider the GCM-RCM combinations as one uncertainty source.
723 The two bias-adjustment methods are considered the second uncertainty source. The ANOVA method provides not only
724 variations in the impact on temperature/precipitation from these two major sources, but also their interaction term. To avoid

725 the bias caused by different sample sizes of the sources, the ANOVA was implemented for a number of subsamples, each of
726 which includes two climate models and two bias correction methods, and then the obtained estimates of subsamples were
727 averaged. For more explanation of the method and equations, please refer to Vetter et al. (2017).

728 Since our implementation of 3DBC conserves the annual changes from EQM, the annual fraction of variance from the ANOVA
729 analysis (Fig. 42-14 and 43-15) is solely dependent on the GCM-RCM combination. On a seasonal scale, the largest contribution
730 to temperature uncertainties still comes from the GCM-RCM combinations. However, for spring and autumn the bias-
731 adjustment contribution can be of similar size, especially in the near future projections. Interactions between the two
732 uncertainty sources are generally small.

733 For precipitation, the contribution to the overall uncertainty from the bias-adjustment methods is larger than the contribution
734 from the climate models for spring and autumn in the near future. Also for the other two seasons, the different contributions
735 are of similar size for the near future. Interestingly, for the far future, the contribution from the climate models is clearly larger
736 than the contribution from the bias-adjustment methods for all seasons. ~~For precipitation,~~ The interactions are larger than for
737 temperature and can reach magnitudes similar to the single contributions. This is an effect of the two bias-adjustment methods
738 resulting in seasonal change signals that differ more for precipitation than temperature, showing that results for temperature
739 from a single bias-adjustment method are more robust than for precipitation. This is especially true for the near future.

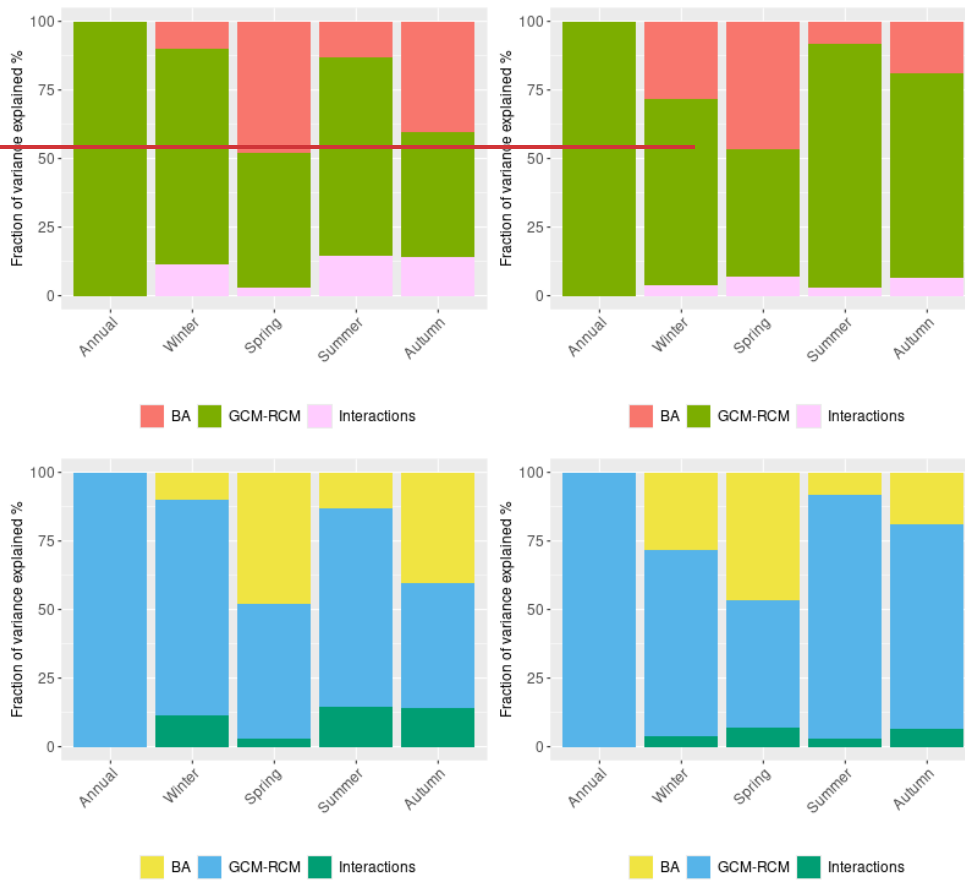


Figure 1214: the fraction of variance in projected temperature changes explained by bias-adjustment methods (BA), GCM-RCM combinations and their interactions for the near-future period (2041–2070, left) and far-future period (2071–2100, right).

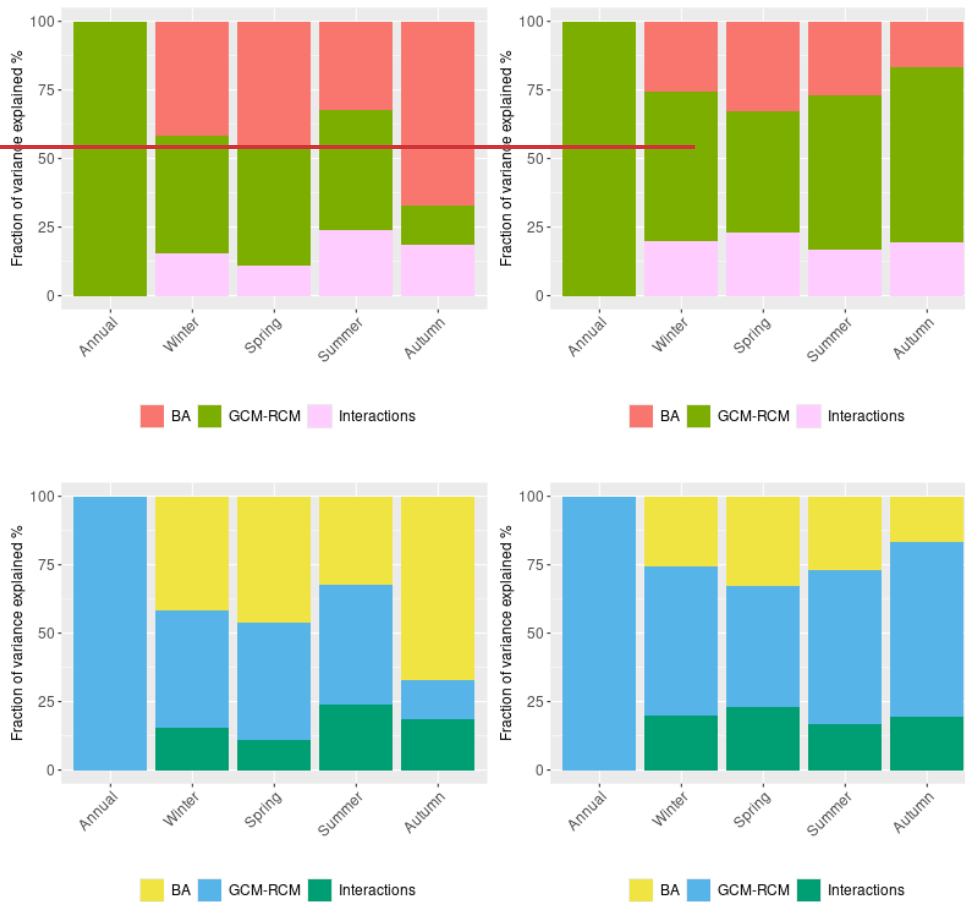


Figure 1315: The same as Fig. 14 but for precipitation, the fraction of variance in projected precipitation changes explained by bias-adjusted methods (BA), GCM-RCM combinations and their interactions for the near-future period (2041–2070, left) and far-future period (2071–2100, right).

Our findings bring new insights into uncertainty attribution for seasonal projections, because most studies on uncertainty attribution are mainly targeted at annual values rather than seasonal ones, e.g. Paz & Willems (2022) and Lafferty & Srivier

(2023). There are only a few uncertainty analyses for seasonal changes, but they did not find larger uncertainty associated with bias-adjustment methods than the variability within the model ensemble (Tong et al., 2021; Zhang et al., 2024). Our results highlight that bias-adjustment methods can be an important uncertainty source for seasonal projections and their seasonal effects should be considered in future studies.

formaterte: Skrift: 10 pkt, Ikke Fet

8 National hydrological projections

8.1 Ensemble means and ranges

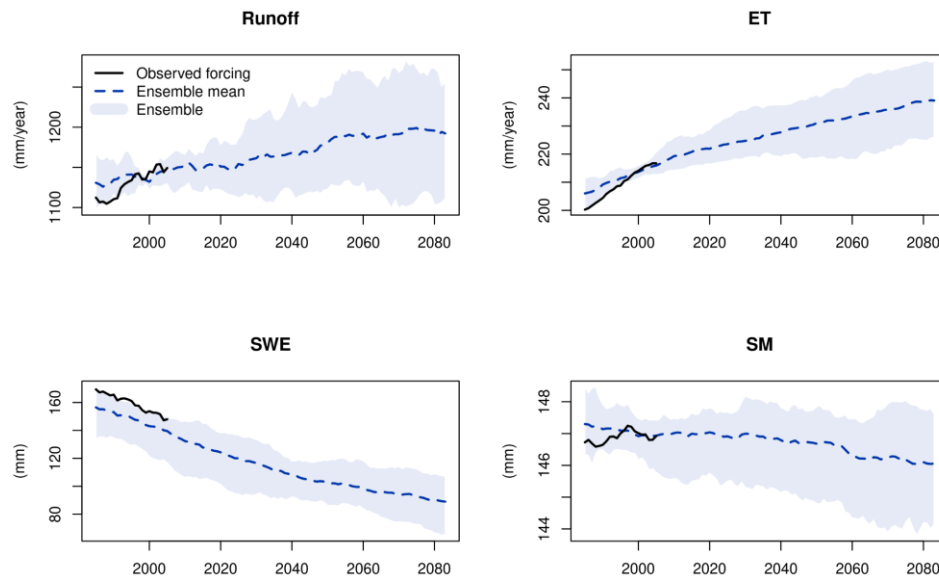
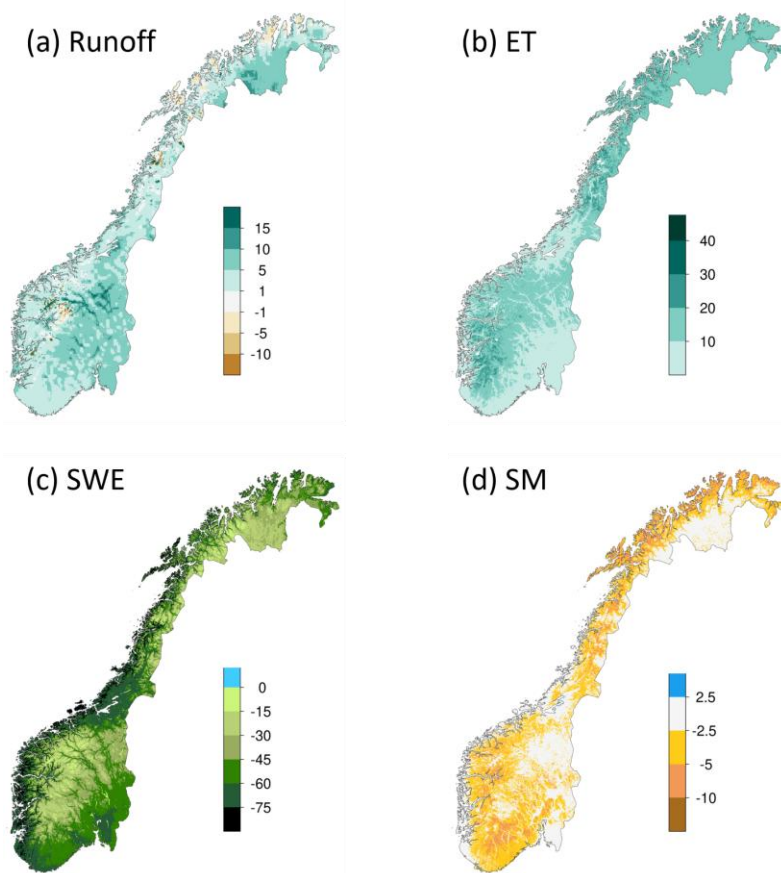


Figure 1416: Simulated 30-year running means of annual runoff, evaporation (ET), mean snow water equivalent (SWE) and mean soil moisture (SM) driven by the ensemble of 20 climate projections (10 GCM-RCMs x 2 bias correction methods) under the RCP4.5 scenario. The black line is the simulated water components driven by the observed forcing data.

762 There are 20 hydrological projections for mainland Norway at 1km spatial resolution with daily time steps under the RCP4.5
763 scenario from the distHBV-COR-BA-2025 dataset. Figure 14-16 shows the projected annual sum/mean of these variables from
764 1971 to 2098 for mainland Norway. Both the ensemble means of runoff and evaporation have an increasing trend while the
765 ensemble means of snow water equivalent and soil moisture trend to decrease towards the end of this century. The simulated
766 runoff, evaporation, and soil moisture driven by the seNorge forcing data (black lines) are generally within the boundary of
767 the 20 simulations in the historical period, and they have a good agreement with the ensemble mean ~~after around~~ the year 2000,
768 ~~indicating good estimates of these variables driven by the bias-adjusted climate projections. In addition, the spread of~~
769 ~~projections is reduced around the year 2000, as the bias-adjusted data matches the statistics of the observations better in the~~
770 ~~training period 1985-2014 than other periods.~~ However, all snow water equivalent simulations are generally underestimated
771 compared with the simulated snow water equivalent driven by the seNorge data, indicating that snow generation is not well
772 reproduced. It is mainly due to inaccurate inter-variable, spatial and temporal dependence between the bias-adjusted
773 atmospheric variables when only the EQM method is used (see section 8.2).

774 Figure 15-17 shows the spatial distribution of the ensemble mean changes in the last scenario period (2071–2100) relative to
775 the reference period (1991–2020). In general, the ~~increase in~~ changes in runoff ~~are is~~ dominant in the whole country, except
776 glacier retreat areas around the glaciers and the coastal areas in the northern part of Norway. The increasing changes are minor
777 (<5%) or moderate (5–10%) in most parts of the country and strong increase in runoff (> 10%) occurs mainly in the glacier
778 areas, lakes and rivers as well as some northernmost areas. Due to the warmer and wetter climate in the future, evaporation is
779 projected to increase in the whole country, especially in western and central Norway. In contrast, the annual mean snow water
780 equivalent will decrease in the whole country in the far future, with a strong decrease (<-75%) along the coast. Note that snow
781 volumes along the coast of Southern Norway are small in today's climate. The absolute decrease in annual mean snow water
782 equivalent is not stronger along the coast than mountainous areas. Soil moisture will decrease in most parts of the country due
783 to the increase in evaporation ~~and earlier snow melt~~, and moderate to strong decreases (<-5%) are mainly found in some
784 southern areas and the coastal regions in the north.



785

786

787

788

Figure 15: ensemble mean changes (%) in annual runoff (a), evaporation (ET) (b), snow water equivalent (SWE) (c) and soil moisture (SM) (d) in the scenario period 2071–2100 relative to the reference period 1991–2020 under the RCP4.5 scenario for mainland Norway.

789

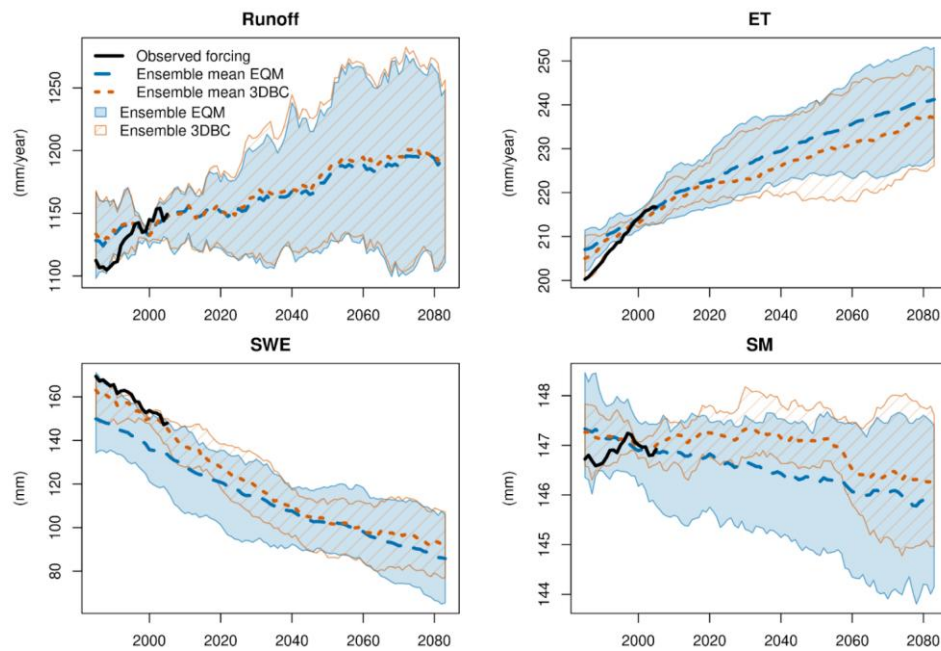
8.2 Effects of the two bias-adjustment methods

790

791

In this section, we provide a general overview of the effects of the bias-adjustment methods on hydrological projections. [Figure 18](#) shows again the projected annual sum/mean of hydrological variables from 1971 to 2098 for mainland Norway, but

792 separating the projections between the two bias-adjustment methods. The results show that the two bias-adjustment methods
793 play a minor role on ensemble means as well as ensemble spread for runoff, evaporation and soil moisture, with the differences
794 between the bias-adjustment methods less than 10 mm/year for runoff and evaporation and less than 1 mm for soil moisture.
795 The ensemble mean of snow water equivalent using the 3DBC method has a better agreement with the results driven by
796 observed forcing data than the ensemble mean using the EQM method, which always leads to underestimation of snow water
797 equivalent in the historical period. In addition, the ensemble spread for snow water equivalent is narrower using 3DBC than
798 EQM, especially before 2040, indicating lower uncertainty of projections using 3DBC. However, it is interesting to see that
799 the snow water equivalent projections do not differ substantially after 2040 between the two bias-adjustment methods, probably
800 due to less snow days in a warming climate. The minor impact of bias-adjustment methods on annual values also leads to
801 similar spatial distributions of the changes in runoff, evaporation and soil moisture, but considerable differences of changes in
802 snow water equivalent are found along the coast and northmost Norway between the bias-adjustment methods (Fig. S3 in
803 Supplementary material).

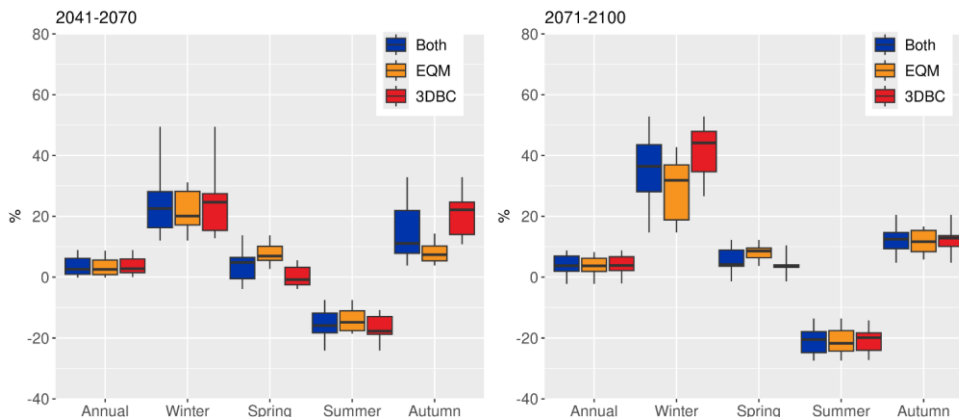


805 Figure 18: The same as Fig. 16, but the projections using different bias-adjustment methods are separated.

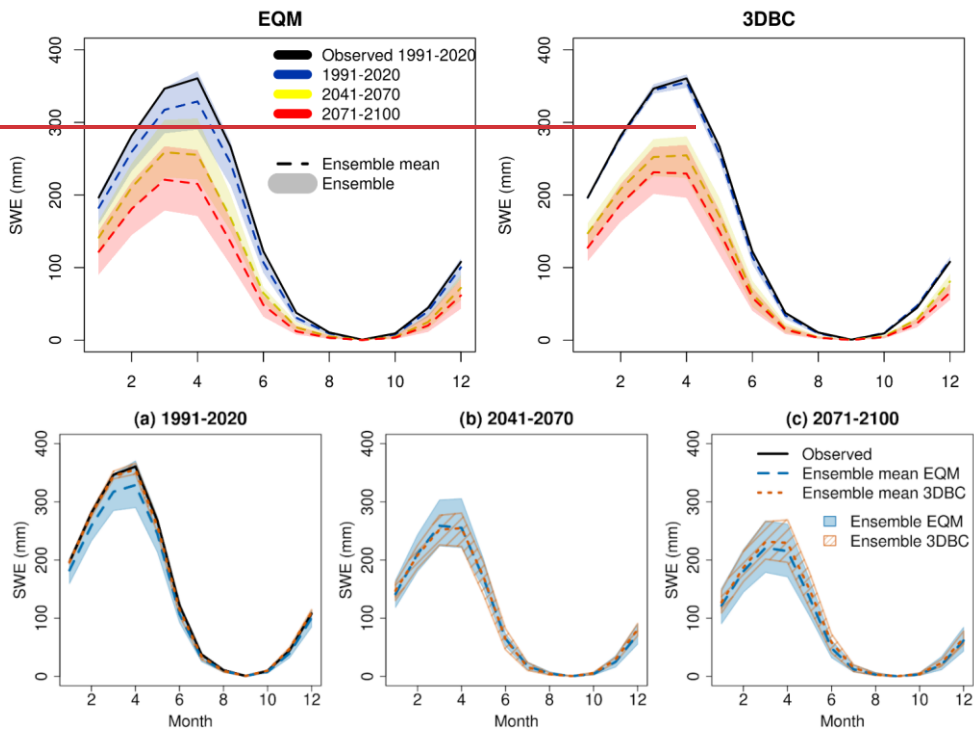
806 Although the bias-adjustment methods affect the annual changes in runoff marginally, they lead to different seasonal runoff
807 changes and their effects vary in scenario periods and seasons. Figure 16-19 shows the seasonal relative changes in runoff
808 including all 20 projections, 10 projections using the EQM bias-adjustment method and 10 projections using the 3DBC method,
809 respectively. The results show that there is a neglectable difference in annual changes between the bias-adjustment methods.
810 However, the bias-adjustment methods lead to different seasonal runoff changes and their effects vary in scenario periods and
811 seasons. In the near future, the largest difference in the ensemble median changes between the bias-adjustment methods is
812 found in autumn (ca. 13%), followed by the difference in spring (ca. 8%), winter (ca. 5%) and summer (ca. 3%). The 3DBC
813 method leads to higher runoff changes in winter and autumn, but lower runoff changes in spring and summer than the EQM
814 method. As a result, the two methods lead to similar changes in annual changes. In the far future, the bias-adjustment methods
815 mainly affect the runoff changes in winter and spring, resulting in a difference in median changes of 12% in winter and 5% in
816 spring. There is almost no difference in median runoff changes between the methods in summer and autumn. These results
817 indicate that the two bias-adjusted methods mainly affect the snow accumulation and melt processes, which occur in autumn,
818 winter and spring in the near future and in winter and spring in the far future. In addition, 3DBC always leads to higher runoff
819 in winter and lower runoff in spring than EQM in both scenario periods.

formaterte: Skrift: 9 pkt

formaterte: Skrift: 9 pkt



820 **Figure 16-19:** relative changes in runoff for different seasons in the scenario periods 2041–2070 (left) and 2071–2100 (right) relative
821 to the reference period 1991–2020 under the RCP4.5 scenario for mainland Norway.
822
823

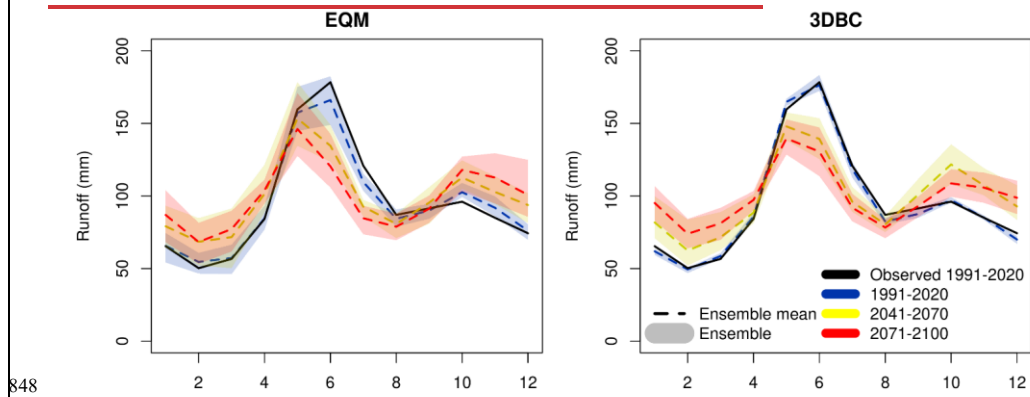


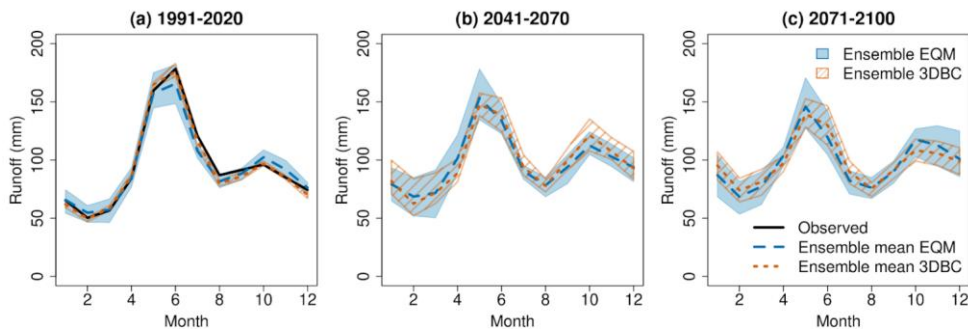
824
825
826 **Figure 2017: Simulated monthly snow water equivalent (SWE) for mainland Norway using the EQM (left) and 3DBC (right) bias-**
827 **adjusted climate projections. Black line: the simulated SWE using observed forcing data in 1991–2020. Blue, yellow and red dash**
828 **lines: the ensemble mean of simulated SWE in different periods, while the blue, yellow and red areas include the ensemble of 10**
829 **projections.**

830 In order to illustrate the effects of the two bias-adjustment methods on snow processes, we compared the monthly snow water
831 equivalent in the historical and scenario periods driven by different bias-adjusted projections as well as the ones driven by the
832 observed forcing data (Fig. 1720). In the historical period, the ensemble mean of monthly snow water equivalent driven by the
833 3DBC bias-adjusted projections agrees well with the simulated one driven by the observed forcing data. The EQM bias-
834 adjusted simulations generally lead to underestimation of monthly snow water equivalent, especially in March and April,
835 similar to the findings by Meyer et al. (2019). In addition, the historical snow simulations using the EQM method vary

836 substantially between climate models, while all bias-adjusted climate projections using the 3DBC method lead to similar
837 monthly SWE, indicating more robust snow projections in the historical period using the 3DBC method than the EQM method.

838 The two bias-adjusted methods also affect the projected changes in snow water equivalent in the scenario periods, especially
839 in the near future. The ensemble mean of monthly snow projections using the 3DBC methods show average decreases of about
840 44 and 55 mm/month in the near and far future periods relative to the reference period respectively, while the ensemble mean
841 using the EQM method decreases by 33 and 50 mm/month on average in the near and far future periods, respectively. It is due
842 to higher snow water equivalent in the historical period and lower snow water equivalent in the near future using the 3DBC
843 bias-adjusted projections than those using the EQM projections. However, the differences in snow water equivalent between
844 the near and far-future periods are smaller using the 3DBC than the EQM method, leading to closer agreement on snow water
845 equivalent changes in the far future between the two methods. The uncertainty bounds of snow projections using the 3DBC
846 method are still smaller than the uncertainty bounds using the EQM method in both future periods, but the differences in
847 uncertainty bounds between the two methods is less substantial than the ones in the historical period.



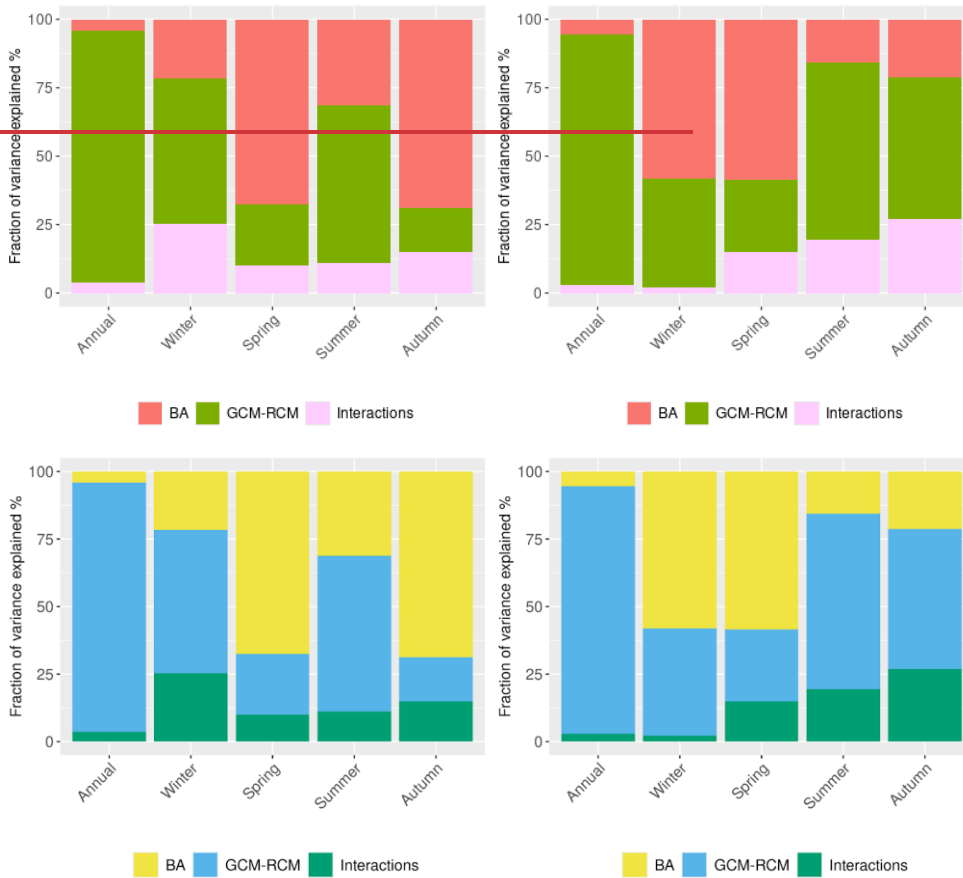


849
850 **Figure 2118: Simulated monthly runoff for mainland Norway using the EQM and 3DBC bias-adjusted climate projections. Black**
851 **line: the simulated runoff using observed forcing data in 1991–2020. Blue, yellow and red dash lines: the ensemble mean of simulated**
852 **runoff in different periods, while the blue, yellow and red areas include the ensemble of 10 projections. The same as Fig. 20 but for**
853 **runoff.**

854 Partly due to different snow simulations, the monthly runoff projections also differ between the two bias-adjustment methods
855 (Fig. 4821). In the historical period, the simulated runoff using the 3DBC bias-adjusted climate simulations also agrees well
856 with the simulated runoff using observed forcing data, while the simulations using the EQM bias-adjusted climate simulations
857 underestimate runoff from June to July that is generated by snow melt, mainly due to less snow storage in winter and spring
858 (Fig. 4720). There is also an overestimate of runoff from October to November using the EQM bias-adjusted climate
859 simulations, indicating that other hydrological processes besides snow are also affected by the inaccurate spatial and temporal
860 correlations of climate variables. Similarly, the runoff simulations using the EQM bias-adjusted climate projections have larger
861 uncertainty bounds than the ones using the 3DBC projections.

862 In the future periods, the runoff projections using the 3DBC method show larger increase and decrease in monthly changes
863 relative to the historical period than using the EQM ones. In addition, the 3DBC bias-adjusted climate projections lead to
864 higher runoff in autumn in the near-future than in the far-future while the EQM projections show contradicting changes.
865 Different from the snow projection uncertainty, the runoff uncertainty using the 3DBC method is not always smaller than the
866 one using the EQM method in all months. In addition, the large runoff uncertainty in the historical and future periods does not
867 lead to large uncertainty of runoff changes. As shown in Fig. 169, the uncertainty bounds of runoff changes using the 3DBC
868 method is not substantially larger than the uncertainty of changes using the EQM method.

869 **8.3 Uncertainty analysis**



870

871

872 **Figure 2249:** the fraction of variance in runoff change projections explained by bias-adjustment methods (BA), GCM-RCM
 873 combinations and their interactions for the near-future period (2041-2070) (left) and far-future period (2071-2100).

874 Similar to temperature and precipitation, we assessed the contribution of the two bias-adjustment methods and GCM-RCM
 875 combinations to the uncertainty in the runoff projections. Figure 49-22 shows the fraction of variance from the ANOVA

876 analysis for the GCM-RCM combinations, bias-adjustment methods and their interactions for the two future periods. For both
877 periods, it is obvious that the climate model combinations contribute to the majority of the annual runoff change variance (>
878 90%). However, the bias-adjustment methods play important roles in the seasonal runoff changes, especially in spring and
879 autumn in the near future and in the winter and spring in the far future, explaining more than 50% of the runoff change variance.
880 For summer, the climate model combinations are always the major uncertainty source, explaining more than 50% of the total
881 runoff change variance. These results highlight the effects of bias-adjustment methods on seasonal runoff change projections.

882 9 Discussion

883 9.1 Limitations of the methodology

884 In this study, we present the whole modelling chain that produces the updated national ensembles of climate and hydrological
885 projections for the new Climate in Norway report CiN-2025 (Dyrørdal et al., 2025). This modelling chain includes selection of
886 emission scenarios and climate models, downscaling and bias-adjustment methods and hydrological models. Although we
887 have made a number of substantial improvements in each component of the modelling chain, there are still limitations and
888 weaknesses in the methodology, which require further development for future climate impact assessments.

889 The first component in the modelling chain is to select appropriate emission scenarios and climate projections from a large
890 ensemble of GCM and RCM outputs manageable throughout the complete chain. As a national climate assessment report
891 following the sixth IPCC report, it would have been ideal to apply the most updated emission scenarios (i.e., the SSPs) and the
892 corresponding climate projections. However, due to the long time needed to make the newest RCM results available within
893 the CORDEX framework and the time limit of the national report, we had to apply the climate projections corresponding to
894 the fifth IPCC report for the low- and median emission scenarios (RCP scenarios). Complements of the national climate
895 projections for SSP emission scenarios are expected in the future to provide up-to-date knowledge on climate change impacts.

896 Since the EURO-CORDEX ensemble for the RCP scenarios is now much larger than for CiN-2015, the climate projections
897 for CiN-2025 are more representative of the full range of climate changes ensembles. However, the restriction to ten models
898 per scenario stemming from the complete modelling chain still partly limits the representativeness of the full possible outcome
899 and model variability. In CiN-2025, this limitation is taken into account for temperature and precipitation using [results from](#)
900 [empirical-statistical downscaling \(ESD\) results from of the complete set of available GCMs, which is not shown in this study.](#)
901 [The ESD results are shown in the CiN-2025 report but not in this study as our focus is on the complete modelling chain. A](#)
902 [detailed description of the ESD method used in CiN-2025 is given in Benestad et al. \(2025\).](#)

903 ~~Additionally,~~ RCMs are still subject to general limitations of model simplifications, such as internal parameterizations and
904 spatial resolution. Further, some technical limitations remain in the RCM outputs, for example, some models provide outputs

905 for 360 days per year, no leap year days or start in 1970 and end in 2098. This brings challenges for impact models and requires
906 pre-processing before bias-adjustment. In addition, the historical period simulated by the RCMs does not cover the current
907 standard normal period (1991–2020). This is a drawback since it is easier for the general public to compare the climate change
908 signals with respect to the climate normal than other non-standard periods (e.g., 1976–2005). Although the use of the first few
909 years from the scenario projections as reference period is not optimal, and the choice of the reference period can lead to
910 different climate changes signals (Liersch et al., 2020), the use of the most recent standard normal period improves the public
911 acceptance and understandability substantially, which is most important for the target users of a national report such as CiN-
912 2025.

913 As the second component of the modelling chain, downscaling and bias-adjustment methods allow presenting projected climate
914 and hydrological changes at a spatial resolution of 1x1 km for the complex topography of Norway. Providing such high
915 resolution data needs high computational costs and makes it challenging to test and apply a large number of bias-adjustment
916 methods. Hence, we only selected EQM as the bias-adjustment method as it is robust for different climatological regimes and
917 well established. The 3DBC method is further applied on the EQM bias-adjusted variables to improve the inter-variable, spatial
918 and temporal dependencies. This multivariate bias-adjustment method indeed improves the hydrological projections,
919 especially for snow simulations, and reduces the uncertainty range, especially in the reference period. However, the 3DBC
920 method (Section 5.23) leads to different climate change signals compared to the original RCM signals on sub-annual scales
921 because it imposes temporal dependency structures on the future projections similar to the ones from the reference datasets.
922 This may be considered a weakness of the approach and more evaluation and development of multivariate bias-adjustment
923 methods are required to further improve the existing methods. As discussed in François et al. (2020), the choice of method
924 may differ from case to case, depending on which statistical properties from the RCMs need to be preserved or corrected.
925 Based on our findings, users of the bias-adjusted data may select the appropriate dataset depending on their needs, or simply
926 consider the two methods being equal, resulting in a broader ensemble.

927 In this study, RCM outputs have firstly been interpolated to the resolution of the observations (1 km) using the nearest-
928 neighbour method and then bias-adjusted on that resolution. However, users should not overinterpret projected changes which
929 are finer than the native RCM resolution (~12.5 km) as the resolving power of the RCM sets the natural lower limit on which
930 local-scale physical processes can be considered. Maraun (2013) has shown that the quantile mapping method cannot resolve
931 this scale mismatch. This effect might be less important for temperature than precipitation as temperature usually has a much
932 higher spatial coherence while precipitation is more subjected to small-scale variability. Although generally both the EQM
933 and the 3DBC methods in our setup do not bring in climate change signals below the RCM resolution, some artifacts might be
934 introduced which do not represent true local, small-scale climate changes.

935 Regarding hydrological models, both the potential evaporation module and glacier modelling have been improved compared
936 to the model used in CiN-2015. The Penman-Monteith method ~~substantially~~ improves ~~the spatial distribution of~~ evaporation

estimates under climate scenarios by considering more climate variables and representing different land cover types (Huang et al., 2026), while the dynamic glacier modelling by DEW successfully avoids unrealistically high runoff from the glacier retreat areas under a warming climate. However, the simulations of DistHBVdistHBV may still suffer equifinality problems due to a large number of calibration parameters, which do not represent the physical characteristics of specific land use and soil types. In addition, we reclassify the soil types into five major groups in order to reduce the number of calibration parameters related to soil processes. This may lead to unreliable simulations for the areas where the soil condition is largely different from the major soil types. Therefore, both the calibration procedure and the spatial representation of soil physical characteristics are expected to improve in the future national applications. ~~The emerging machine learning techniques have been successfully used to calibrate one distributed land surface model (Farahani et al., 2025), and they are expected to play more important roles in hydrological model calibrations.~~

Last but not least, vegetation types and characteristics are static in our hydrological modelling under climate change scenarios, but the changes in vegetation characteristics are expected under a warming climate. Huang et al. (2025a) assessed the effects of forest growth and forest management on water resources in six Norwegian catchments under the RCP2.6 and RCP4.5 emission scenarios. They found that forest growth would offset the increase in runoff in the catchments, where the deciduous forest is dominant. It implies that the runoff in the deciduous forest areas, especially in North Norway, may be overestimated in our present runoff projections. For the next generation CiN report, the land use and vegetation change scenarios should be included in the hydrological modelling if such scenarios are available.

9.2 Comparison of results between the old and new national reports

The improved modelling chain generated updated climate and hydrological projections for Norway, which resulted in slightly different climate change signals and climate impacts compared to the analysis in the old national report. Under the RCP4.5 scenario, the projections for the old and new national reports agree on the direction of change, but CiN-2025 projections display a smaller increase in annual temperature (ensemble mean of 2.0 °C) and precipitation (ensemble mean of 6%) than the ensemble means in CiN-2015 (2.7 °C and 8% increase in temperature and precipitation respectively) at the end of the century. In addition, the ensemble spread in CiN-2025 is narrower than in CiN-2015, indicating more robust climate change signals. However, these differences are caused not only by the new selection of climate models, but also by the selection of the reference period. In CiN-2015, 1971–2000 was used as the reference period while in CiN-2025, it is 1991–2020. As temperature has already risen considerably in recent decades in Norway, annual mean temperature is higher in 1991–2020 than in 1971–2000, and the differences in temperature between the periods 2071–2100 and 1991–2020 are consequently more moderate than those between 2071–2100 and 1971–2000. In contrast, a larger increase in runoff is seen in CiN-2025 projections than in the previous one, mainly due to the improved evapotranspiration routine in the hydrological model (Huang et al., 2026).

Formatert: Mellomrom Etter: Automatisk

formaterte: Engelsk (USA)

formaterte: Engelsk (USA)

967 Another major difference between the old and new national report is that CiN-2025 selected SSP3-7.0 as the high-emission
968 scenario, which assumes lower emission than RCP8.5 used in CiN-2015. Under SSP3-7.0, the ensemble mean increases in
969 annual mean temperature, precipitation and runoff are 3.4 °C, 11% and 10% in 2071-2100 relative to 1991-2020, respectively
970 (Fig. S4, S5 and S16 in Supplementary materials). These increases are also smaller than the ones in 2071-2100 relative to
971 1971-2000 under the RCP8.5 scenario, shown in the old national report. Hence, users who have made computations based on
972 the CiN-2015 projections, should notice these differences and justify whether their computations should be updated or not.

formaterte: Engelsk (USA)

973 9.3 Results from The effects of bias-adjustment methods under the high-emission scenario SSP3-7.0

974 This paper comprehensively compared the two bias-adjustment methods applied to EURO-CORDEX RCP4.5 simulations and
975 found that the two methods can lead to considerable differences in seasonal changes and snow simulations under the moderate-
976 emission scenario. However, the impact of the bias-adjustment methods may not only vary between climate models and future
977 periods but also between emission scenarios. Thus, results for the same comparison between the two bias-adjustment methods
978 under SSP3-7.0 are included in the Supplementary material (Figures S6-S19). Although the magnitudes of the projected
979 changes between SSP3-7.0 and RCP4.5 differ, the general effects and differences between the two bias-adjustment methods
980 are similar. One interesting aspect is a generally better agreement of the SSP3-7.0 ensemble mean temperature and precipitation
981 with the observed values than in the RCP4.5 simulations during the reference period (Fig. S4).

formaterte: Engelsk (USA)

formaterte: Engelsk (USA)

formaterte: Engelsk (USA)

982 For hydrological projections, 3DBC still provides better historical simulations than EQM under the SSP3-7.0 scenario, but the
983 difference in future projections varies between the bias-adjustment methods and seasons. Considerable differences of ensemble
984 mean changes in runoff are found in all seasons in the near future and in winter in the far future. The ensemble spreads of
985 monthly projections for snow water equivalent and runoff are similar between 3DBC and EQM for almost all months,
986 indicating that 3DBC does not help to reduce the projection uncertainty substantially under extremely warm conditions.

formaterte: Engelsk (USA)

formaterte: Engelsk (USA)

formaterte: Engelsk (USA)

987 9.2.4 Application

988 Despite the limitations mentioned above, the COR-BA-2025 and distHBV-COR-BA-2025 datasets generated by the presented
989 modelling chain provide the most updated, comprehensive and detailed hydrometeorological projections for mainland Norway.
990 These national projections serve as the scientific basis for research on climate change impacts in Norway. The gridded
991 hydrometeorological projections from CiN-2015 have already been used to derive new indices for specific application, e.g.
992 snow-dependent tourism (Kuya et al., 2024; Mayer et al., 2023), reindeer husbandry (Hanssen-Bauer et al., 2022), frost decay
993 exposure on building projects (Gaarder et al., 2024) and road maintenance (Nilsen et al., 2021). In addition to impact modellers,
994 who represent an advanced user group, NCCS aims at providing tailored information for practical climate adaptation. Products
995 derived from the national projections have also been widely used in local planning, mainly because government guidelines
996 (Norwegian Government, 2024) required municipalities to take climate change into account in planning. Climate factsheets

997 (Hisdal et al., 2021) provided the most relevant information to guide the climate adaptation work, and were pointed out as a
998 core reference in government guidelines. See Nilsen et al. (2022) for an overview of the steps from climate model output to
999 actionable climate information.

1000 Besides the possibility to update existing applications that used the gridded dataset from CiN-2015, [the new COR-BA-2025](#)
1001 and [distHBV-COR-BA-2025 datasets](#) provide additional variables, such as wind speed, pressure, evaporation, radiation and
1002 relative humidity, [each bias-adjusted both with EQM and 3DBC](#). This improves the utility of the dataset for e.g., ecological
1003 modelling (see Pirk et al., 2023 for an example). It is expected that the new dataset will facilitate use in an even wider range
1004 of applications in the coming years, for climate change impacts on e.g., glaciers, drought, landslides and water availability.
1005 Further work will involve user groups such as municipal planners to co-create climate services based on the
1006 hydrometeorological projections presented.

1007 [In principle, we suggest using the full ensemble projections with both bias-adjustment methods to account for the uncertainty](#)
1008 [of the whole modelling chain. But in practice, users may want to select a subset of climate models and one bias-adjustment](#)
1009 [method to reduce the computational cost of further applications. As the users may be only interested in parts of Norway and](#)
1010 [the performance of climate models and bias-adjustment methods vary in space and time, we are not able to give a](#)
1011 [straightforward suggestion on the subset of climate models and bias-adjustment methods based on the national analysis.](#)
1012 [However, the methodology as well as the analysis in this paper provides examples of selecting models and bias-adjustment](#)
1013 [methods. In order to select a subset of climate models, the users can analyze the climate signals for their study area and periods](#)
1014 [as in Fig. 3 and then select the models based on the study purpose, e.g., studies aiming to assess the driest and warmest climate](#)
1015 [conditions or the wettest and coldest conditions in the near or far future. Based on the selected models, the users can further](#)
1016 [assess the seasonal trends for their study area and periods using both EQM and 3DBC projections as in Fig. 6. If the trends are](#)
1017 [comparable between the two bias-adjustment methods, the 3DBC adjusted projections can be preferred, especially when the](#)
1018 [study is focused on seasonal changes and snow processes. Otherwise, we strongly recommend to use the projections adjusted](#)
1019 [by EQM and 3DBC to account for the uncertainty of bias-adjustment methods.](#)

1020 Finally, we should note that the gridded datasets [distHBV-COR-BA-2025](#) are not designed to use for flood indices, or climate
1021 change allowances for floods because [distHBV](#) was calibrated against many catchments simultaneously. Instead, the outputs
1022 from specific flood models should be used (Lawrence, 2020; Carr et al., 2023). The flood models include two lumped
1023 hydrological models and were calibrated against observed discharges for each catchment separately. Hence, the flood models
1024 produce more reliable estimates of high (and low) flow for specific catchments.

1025 10 Conclusions

1026 In this study, we present the whole modelling chain behind the production of updated national ensembles of climate and
1027 hydrological projections for the official “Climate in Norway” assessment report. We also provide insight into the
1028 hydrometeorological projections, which we termed COR-BA-2025 (standing for CORDEX-Bias Adjusted, updated in 2025)
1029 for climate projections and distHBV-COR-BA-2025 for hydrological projections, and analyse their uncertainties. The
1030 modelling chain (Fig. 2) includes the selection of GCM-RCM combinations for Norway from a large ensemble of EURO-
1031 CORDEX simulations, the application of two bias-adjustment methods and distributed hydrological modelling including a
1032 physically-based potential evaporation approach and a dynamic glacier model. Compared to the previous national assessment
1033 report, the new climate projections are considered more representative for Norway due to a larger ensemble of EURO-
1034 CORDEX simulations taken into account and a systematic analysis of the projections.

1035 A multivariate bias-adjustment method has been applied for the first time over the whole of Norway for the complete
1036 atmospheric dataset consisting of nine variables. This new method leads to more consistent data in space, time and between
1037 variables, and to more robust hydrological simulations than the univariate empirical quantile mapping method (especially for
1038 snow and in the reference period), but it does not preserve climate change signals on a sub-annual scale. However, the
1039 uncertainty ranges of runoff change projections are not significantly different between the two bias-adjustment methods,
1040 especially at the annual scale. An uncertainty analysis shows that the climate projections are the major source of uncertainty
1041 for annual runoff change, while the selection of the bias-adjustment method plays an important role on seasonal changes.

1042 Despite the advancement in the presented methodologies and modelling chain, there is still room for further improvement in
1043 future climate impact assessment studies. Currently we foresee that additional emission scenarios and GCM-RCM
1044 combinations from the EURO-CORDEX initiative will be evaluated and the bias-adjustment methods will be further developed
1045 to overcome the current limitations. In addition, the calibration procedure and the calibration parameters in the hydrological
1046 modelling will be further improved using advanced machine learning techniques. If possible, the land use and vegetation
1047 changes scenarios should also be considered in hydrological modelling.

1048 The methodological description provided here serves as core knowledge for any further application of the gridded products,
1049 which are expected to be used in a wide range of climate impact assessments and development of climate adaptation strategies
1050 in Norway. We have thrived to meet the FAIR principles (Wilkinson et al., 2016) for data management. Thus, the complete
1051 COR-BA-2025 and distHBV-COR-BA-2025 datasets (Wong et al. 2025) are findable and accessible through the Arctic Data
1052 Centre (adc.met.no) at <https://doi.org/10.21343/0k90-6w67>. The data is stored in NetCDF format following the attribute
1053 convention for data discovery (ACDD version 1-3, https://wiki.esipfed.org/Attribute_Convention_for_Data_Discovery_1-3)
1054 and the climate and forecast metadata conventions (CF version 1.10, Eaton et al., 2022). The code and data are reusable, being
1055 open source with non-restrictive licenses.

1056 **Code availability**

1057 The code of [DistHBVdistHBV](https://doi.org/10.5281/zenodo.17531118) is available at <https://doi.org/10.5281/zenodo.17531118> (Beldring, 2025a)

1058 The code of DEW is available at <https://doi.org/10.5281/zenodo.17530242>, (Beldring, 2025b)

1059 The R source code of the 3DBC implementation used in this work is available at <https://doi.org/10.5281/zenodo.15260334>
1060 (Dobler, 2025).

1061 EQM implementation used the functions *fitQmapQUANT* and *doQmapQUANT* from R package *qmap* which is available at
1062 <https://doi.org/10.32614/CRAN.package.qmap> (Gudmundsson, 2025).

1063 **Data availability**

1064 The **COR-BA-2025** and **distHBV-COR-BA-2025** bias-adjusted daily high-resolution climate and hydrological projections
1065 for Norway are freely available at the Arctic Data Centre (adc.met.no) under <https://doi.org/10.21343/0k90-6w67> (Wong et
1066 al., 2025).

1067 The reference datasets used in the modelling chain are available at <https://doi.org/10.21343/gbq0-4t97> (Huang et al., 2025b).

1068 **Author contribution**

1069 SM, SLS, TL, WKW and AD performed the analysis of climate model selections and collected the RCM data. WKW and AD
1070 designed the bias-adjustment experiments and methods and carried them out. IH modified the model code [DistHBVdistHBV](https://doi.org/10.5281/zenodo.17531118)
1071 and IH and SH performed the simulations. SB and KM developed the model code DEW, designed the experiments of DEW
1072 and GR performed the simulations. SH prepared the manuscript with contributions from all co-authors. AVD, HOH, IBN and
1073 SJB coordinated the whole project.

1074 **Competing interests**

1075 The authors declare that they have no conflict of interest.

1076 **Acknowledgement**

1077 We acknowledge the World Climate Research Programme, the CORDEX Science Advisory Team (SAT) - coordinating body
1078 of CORDEX, and the Working Group on Coupled Modelling (WGCM) - responsible panel for CMIP5 and CMIP6. We thank

1079 the CORDEX climate modeling groups (listed in Table 1 [and S1](#)) for producing and making available their model output,
1080 CMIP5 [and CMIP6](#) for providing the driving data, the Earth System Grid Federation (ESGF) for providing access, and the
1081 multiple funding agencies who support CORDEX, CMIP and ESGF.

1082 **Financial support**

1083 This article was funded by the Norwegian Centre for Climate Services, and thus supported by the Norwegian Environment
1084 Agency and the Ministry of Climate and Environment in addition to in-kind contributions from the Norwegian Water
1085 Resources and Energy Directorate, NORCE and the Norwegian Meteorological Institute.

1086 **References**

1087 Ahlstrøm, A., Bjørkelo, K., and Frydenlund, J.: AR5 klassifikasjonssystem - klassifikasjon av arealressurser, Skog og
1088 landskap, rapport nr. 6/2014, 38 pp., <http://hdl.handle.net/11250/2440173>, 2014.

1089 Alifu, H., Hirabayashi, Y., Imada, Y., and Shiogama, H.: Enhancement of river flooding due to global warming, *Sci Rep*, 12,
1090 20687, <https://doi.org/10.1038/s41598-022-25182-6>, 2022.

1091 Andreassen, L. M., Huss, M., Melvold, K., Elvehøy, H. og Winsvold, S. H.: Ice thickness measurements and volume
1092 estimates for glaciers in Norway. *Journal of Glaciology*, 61(228), 763-775. <https://doi.org/10.3189/2015JoG14J161>, 2015.

1093 [Astagneau, P. C., Wood, R. R., Vrac, M., Kotlarski, S., Vaittinada Ayar, P., François, B., and Brunner, M. I.: Impact of bias
1094 adjustment strategy on ensemble projections of hydrological extremes. *Hydrol. Earth Syst. Sci.*, 29, 5695–5718,
1095 <https://doi.org/10.5194/hess-29-5695-2025>, 2025.](#)

1096 [Ayar, P. V., Vrac, M., Bastin, S., Carreau, J., Déqué, M., and Gallardo, C.: Intercomparison of statistical and dynamical
1097 downscaling models under the EURO and MED CORDEX initiative framework: present climate evaluations, *Clim Dyn*, 46,
1098 1301–1329, <https://doi.org/10.1007/s00382-015-2647-5>, 2016.](#)

1099 Beck, H. E., Zimmermann, N. E., McVicar, T. R., Vergopolan, N., Berg, A., and Wood, E. F.: Present and future Köppen-
1100 Geiger climate classification maps at 1-km resolution, *Sci Data*, 5, 180214, <https://doi.org/10.1038/sdata.2018.214>, 2018.

1101 Beldring, S.: Distributed element water balance model system. *Norwegian Water Resources and Energy Directorate, Report*
1102 *no. 4/2008*, 40 pp. https://publikasjoner.nve.no/report/2008/report2008_04.pdf
1103 https://github.com/DistributedElementWaterModel/Version_3.03, 2008.

1104 Beldring, S.: nve-sbe/DistributedHbv: v_1 (v_1), Zenodo, <https://doi.org/10.5281/zenodo.17531118>, 2025a.

Feltkode endret

Feltkode endret

1105 [Beldring, S.: DistributedElementWaterModel/Version_3.03: v 1 \(v 1\), Zenodo, <https://doi.org/10.5281/zenodo.17530242>,](#)
1106 2025b.

1107 [Beldring, S., Engeland, K., Holmqvist, E., Pedersen, A.I., Ruan, G., Veie, C.A. and Cabrol, J.: *Avrenningskart for Norge 1991–*
1108 *2020. NVE-rapport nr. 36/2022*, \[https://publikasjoner.nve.no/rapport/2022/rapport2022_36.pdf\]\(https://publikasjoner.nve.no/rapport/2022/rapport2022_36.pdf\), 2022.](#)

1109 Beldring, S., Engeland, K., Roald, L. A., Sælthun, N. R., and Voksø, A.: Estimation of parameters in a distributed precipitation-
1110 runoff model for Norway, *Hydrology and Earth System Sciences*, 7, 304–316, <https://doi.org/10.5194/hess-7-304-2003>, 2003.

1111 [Benestad, R. E., Parding, K. M., and Dobler, A.: Downscaling the probability of heavy rainfall over the Nordic countries,](#)
1112 [Hydrol. Earth Syst. Sci., 29, 45–65, <https://doi.org/10.5194/hess-29-45-2025>, 2025.](#)

1113 [Bergström, S.: The HBV-model. V.P. Singh \(Ed.\), *Computer Models of Watershed Hydrology*, Water resources publications,](#)
1114 [pp. 443–476, 1995.](#)

1115 Bremnes, J. B.: Probabilistic wind power forecasts using local quantile regression, *Wind Energy*, 7, 47–54,
1116 <https://doi.org/10.1002/we.107>, 2004.

1117 Bright, R. M., Eisner, S., Lund, M. T., Majasalmi, T., Myhre, G., and Astrup, R.: Inferring Surface Albedo Prediction Error
1118 Linked to Forest Structure at High Latitudes, *Journal of Geophysical Research: Atmospheres*, 123, 4910–4925,
1119 <https://doi.org/10.1029/2018JD028293>, 2018.

1120 [Bürger, G., Sobie, S. R., Cannon, A. J., Werner, A. T., and Murdock, T. Q.: Downscaling Extremes: An Intercomparison of](#)
1121 [Multiple Methods for Future Climate, *Journal of Climate*, 26, 3429–3449, <https://doi.org/10.1175/JCLI-D-12-00249.1>, 2013.](#)

1122 Carr, S., Lawrence, D., Skaugen, T., and Wong, W. K.: Projected future changes in peak flows and implications for climate
1123 change allowances, NVE report nr. 26/2023, The Norwegian Water Resources and Energy Directorate, Oslo, Norway,
1124 https://publikasjoner.nve.no/rapport/2023/rapport2023_26.pdf, 2023.

1125 Cannon, A.J., Sobie, S.R. and Murdock, T.Q.: Bias Correction of GCM Precipitation by Quantile Mapping: How Well Do
1126 Methods Preserve Changes in Quantiles and Extremes? *Journal of Climate*, 28, 6938–6959, [https://doi.org/10.1175/JCLI-D-](https://doi.org/10.1175/JCLI-D-14-00754.1)
1127 [14-00754.1](#), 2015.

1128 CH2018: CH2018 – Climate Scenarios for Switzerland, Technical Report. National Centre for Climate Services, Zürich, 271
1129 pp, ISBN: 978-3-9525031-4-0, 2018.

formaterte: Norsk (bokmål)

formaterte: Norsk (bokmål)

formaterte: Norsk (bokmål)

Feltkode endret

Feltkode endret

Feltkode endret

formaterte: Engelsk (USA)

1130 Chinita, M. J., Richardson, M., Teixeira, J., and Miranda, P. M. A.: Global mean frequency increases of daily and sub-daily
1131 heavy precipitation in ERA5, *Environ. Res. Lett.*, 16, 074035, <https://doi.org/10.1088/1748-9326/ac0caa>, 2021.

1132 Dalelane, C., Früh, B., Steger, C., and Walter, A.: A Pragmatic Approach to Build a Reduced Regional Climate Projection
1133 Ensemble for Germany Using the EURO-CORDEX 8.5 Ensemble, <https://doi.org/10.1175/JAMC-D-17-0141.1>, 2018.

1134 DCCEEW: National Climate Risk Assessment: Methodology. Department of Climate Change, Energy, the Environment and
1135 Water, <https://www.dcceew.gov.au/climate-change/publications/national-climate-risk-assessment>, 2023.

1136 Dobler, A.: doblerrone/3DBC: Version 2023 (Versjon v2023), Zenodo, <https://doi.org/10.5281/zenodo.15260335>, 2025.

1137 Dobrowski, S. Z., Abatzoglou, J. T., Greenberg, J. A., and Schladow, S. G.: How much influence does landscape-scale
1138 physiography have on air temperature in a mountain environment?, *Agricultural and Forest Meteorology*, 149, 1751–1758,
1139 <https://doi.org/10.1016/j.agrformet.2009.06.006>, 2009.

1140 Doherty, J. and Skahill, B. E.: An advanced regularization methodology for use in watershed model calibration, *Journal of*
1141 *Hydrology*, 327, 564–577, <https://doi.org/10.1016/j.jhydrol.2005.11.058>, 2006.

1142 Dunn, R. J. H., Alexander, L. V., Donat, M. G., Zhang, X., Bador, M., Herold, N., Lippmann, T., Allan, R., Aguilar, E., Barry,
1143 A. A., Brunet, M., Caesar, J., Chagnaud, G., Cheng, V., Cinco, T., Durre, I., de Guzman, R., Htay, T. M., Wan Ibadullah, W.
1144 M., Bin Ibrahim, M. K. I., Khoshkam, M., Kruger, A., Kubota, H., Leng, T. W., Lim, G., Li-Sha, L., Marengo, J., Mbatha, S.,
1145 McGree, S., Menne, M., de los Milagros Skansi, M., Ngwenya, S., Nkrumah, F., Oonariya, C., Pabon-Caicedo, J. D., Panthou,
1146 G., Pham, C., Rahimzadeh, F., Ramos, A., Salgado, E., Salinger, J., Sané, Y., Sopaheluwakan, A., Srivastava, A., Sun, Y.,
1147 Timbal, B., Trachow, N., Trewin, B., van der Schrier, G., Vazquez-Aguirre, J., Vasquez, R., Villarroel, C., Vincent, L., Vischel,
1148 T., Vose, R., and Bin Hj Yussof, M. N.: Development of an Updated Global Land In Situ-Based Data Set of Temperature and
1149 Precipitation Extremes: HadEX3, *Journal of Geophysical Research: Atmospheres*, 125, e2019JD032263,
1150 <https://doi.org/10.1029/2019JD032263>, 2020.

1151 Dyrddal, A.V., Bakke, S.J., Hanssen-Bauer, I., Mayer, S., Nilsen, I.B., Nilsen, J.E.Ø., Paasche, Ø., Saloranta, T., Årthun, M.
1152 [editors]: Klima i Norge – kunnskapsgrunnlag for klimatilpasning oppdatert i 2025 (“Climate in Norway – knowledge base
1153 for climate adaptation updated in 2025”), NCCS Report 1/2025, Norwegian Centre for Climate Services, Oslo, Norway. (In
1154 Norwegian.). <https://doi.org/10.60839/4rgq-nn84>, 2025.

1155 Eaton, B., Gregory, J., Drach, B., Taylor, K., Hankin, S., Caron, J., Signell, R., Bentley, P., Rappa, G., Höck, H., Pamment,
1156 A., Juckes, M., Raspaud, M., Blower, J., Horne, R., Whiteaker, T., Blodgett, D., Zender, C., Lee, D., Hassell, D., Snow, A. D.,

Feltkode endret

1157 Kölling, T., Allured, D., Jelenak, A. Soerensen, A. M., Gaultier, L., Herlédan, S.: NetCDF Climate and Forecast (CF) Metadata
1158 Conventions (1.10). CF Community. <https://doi.org/10.5281/zenodo.14275561>, 2022.

1159 EEA (European Environment Agency): Energy Performance of Buildings Directive.
1160 [https://energy.ec.europa.eu/topics/energy-efficiency/energy-performance-buildings/energy-performance-buildings-](https://energy.ec.europa.eu/topics/energy-efficiency/energy-performance-buildings/energy-performance-buildings-directive_en)
1161 [directive_en](https://energy.ec.europa.eu/topics/energy-efficiency/energy-performance-buildings/energy-performance-buildings-directive_en), last access: 19 August 2025.

1162 ~~Erlandsen, H. B., Tallaksen, L. M., and Kristiansen, J.: Merits of novel high-resolution estimates and existing long-term~~
1163 ~~estimates of humidity and incident radiation in a complex domain, Earth System Science Data, 11, 797–821,~~
1164 ~~<https://doi.org/10.5194/essd-11-797-2019>, 2019.~~

1165 ~~Erlandsen, H. B., Parding, K. M., Benestad, R., Mezghani, A., and Pontoppidan, M.: A Hybrid Downscaling Approach for~~
1166 ~~Future Temperature and Precipitation Change, <https://doi.org/10.1175/JAMC-D-20-0013.1>, 2020.~~

1167 Erlandsen, H. B., Beldring, S., Eisner, S., Hisdal, H., Huang, S., and Tallaksen, L. M.: Constraining the HBV model for robust
1168 water balance assessments in a cold climate, Hydrology Research, 52, 356–372, <https://doi.org/10.2166/nh.2021.132>, 2021.

1169 Eum, H.-I., Gupta, A., and Dibike, Y.: Effects of univariate and multivariate statistical downscaling methods on climatic and
1170 hydrologic indicators for Alberta, Canada, Journal of Hydrology, 588, 125065, <https://doi.org/10.1016/j.jhydrol.2020.125065>,
1171 2020.

1172 Eyring, V., Bony, S., Meehl, G. A., Senior, C. A., Stevens, B., Stouffer, R. J., and Taylor, K. E.: Overview of the Coupled
1173 Model Intercomparison Project Phase 6 (CMIP6) experimental design and organization, Geoscientific Model Development,
1174 9, 1937–1958, <https://doi.org/10.5194/gmd-9-1937-2016>, 2016.

1175 ~~Farahani, M. A., Wood, A. W., Tang, G., and Mizukami, N.: Calibrating a large domain land/hydrology process model in the~~
1176 ~~age of AI: the SUMMA CAMELS experiments, EGUsphere, 1–35, <https://doi.org/10.5194/egusphere-2025-38>, 2025.~~

1177 Fischer, A. M., Strassmann, K. M., Croci-Maspoli, M., Hama, A. M., Knutti, R., Kotlarski, S., Schär, C., Schnadt Poberaj, C.,
1178 Ban, N., Bavay, M., Beyerle, U., Bresch, D. N., Brönnimann, S., Burlando, P., Casanueva, A., Fatichi, S., Feigenwinter, I.,
1179 Fischer, E. M., Hirschi, M., Liniger, M. A., Marty, C., Medhaug, I., Peleg, N., Pickl, M., Raible, C. C., Rajczak, J., Rössler,
1180 O., Scherrer, S. C., Schwierz, C., Seneviratne, S. I., Skelton, M., Sørland, S. L., Spirig, C., Tschurr, F., Zeder, J., and Zubler,
1181 E. M.: Climate Scenarios for Switzerland CH2018 – Approach and Implications, Climate Services, 26, 100288,
1182 <https://doi.org/10.1016/j.cliser.2022.100288>, 2022.

- 1183 François, B., Vrac, M., Cannon, A. J., Robin, Y., and Allard, D.: Multivariate bias corrections of climate simulations: which
 1184 benefits for which losses?, *Earth System Dynamics*, 11, 537–562, <https://doi.org/10.5194/esd-11-537-2020>, 2020.
- 1185 Franke, J.: Rainfall complexity in mountains, *Nat. Clim. Chang.*, 14, 1223–1223, [https://doi.org/10.1038/s41558-024-02209-](https://doi.org/10.1038/s41558-024-02209-6)
 1186 [6](https://doi.org/10.1038/s41558-024-02209-6), 2024.
- 1187 Frei, C., Christensen, J. H., De'que', M., Jacob, D., Jones, R. G., and Vidale, P. L.: Daily precipitation statistics in regional
 1188 climate models: Evaluation and intercomparison for the European Alps. *J. Geophys. Res.*, 108, 4124,
 1189 <https://doi.org/10.1029/2002JD002287>, 2003.
- 1190 Gaarder, J.E., Tajet, H.T.T., Dobler, A., Hygen, H.O. and Kvande, T.: Future Climate Projections and Uncertainty Evaluations
 1191 for Frost Decay Exposure Index in Norway. *Buildings*, 14(9), p.2873, <https://doi.org/10.3390/buildings14092873>, 2024
- 1192 Golding, N., Lambkin, K., Wilson, L., Troch, R. D., Fischer, A. M., Hygen, H. O., Hama, A. M., Dyrndal, A. V., Jamsin, E.,
 1193 Termonia, P., and Hewitt, C.: Developing national frameworks for climate services: Experiences, challenges and learnings
 1194 from across Europe, *Climate Services*, 37, 100530, <https://doi.org/10.1016/j.cliser.2024.100530>, 2025.
- 1195 Gjertsen, A.K. and Nilsen, J.E.: SAT-SKOG: Et skogkart basert på tolking av satellittbilder. Skog og landskap, rapport nr.
 1196 23/2012, 54 pp, <http://hdl.handle.net/11250/2453917> 2012.
- 1197 Gu, G. and Adler, R. F.: Spatial Patterns of Global Precipitation Change and Variability during 1901–2010,
 1198 <https://doi.org/10.1175/JCLI-D-14-00201.1>, 2015.
- 1199 Gudmundsson, L.: qmap: Statistical Transformations for Post-Processing Climate Model Output, version 1.0-6,
 1200 <https://doi.org/10.32614/CRAN.package.qmap>, 2025.
- 1201 Gudmundsson, L., Bremnes, J. B., Haugen, J. E., and Engen-Skaugen, T.: Technical Note: Downscaling RCM precipitation to
 1202 the station scale using statistical transformations – a comparison of methods, *Hydrology and Earth System Sciences*,
 1203 16, 3383–3390, <https://doi.org/10.5194/hess-16-3383-2012>, 2012.
- 1204 Gudmundsson, L., Boulange, J., Do, H. X., Gosling, S. N., Grillakis, M. G., Koutroulis, A. G., Leonard, M., Liu, J., Müller
 1205 Schmied, H., Papadimitriou, L., Pokhrel, Y., Seneviratne, S. I., Satoh, Y., Thiery, W., Westra, S., Zhang, X., and Zhao, F.:
 1206 Globally observed trends in mean and extreme river flow attributed to climate change, *Science*, 371, 1159–1162,
 1207 <https://doi.org/10.1126/science.aba3996>, 2021.
- 1208 Gutiérrez, J. M., Maraun, D., Widmann, M., Huth, R., Hertig, E., Benestad, R., Roessler, O., Wibig, J., Wilcke, R., Kotlarski,
 1209 S., San Martín, D., Herrera, S., Bedia, J., Casanueva, A., Manzanar, R., Iturbide, M., Vrac, M., Dubrovsky, M., Ribalaygua,

Feltkode endret

Feltkode endret

1210 J., Pórtoles, J., Ráty, O., Räisänen, J., Hingray, B., Raynaud, D., Casado, M. J., Ramos, P., Zerenner, T., Turco, M., Bosshard,
1211 T., Štěpánek, P., Bartholy, J., Pongracz, R., Keller, D. E., Fischer, A. M., Cardoso, R. M., Soares, P. M. M., Czernecki, B.,
1212 and Pagé, C.: An intercomparison of a large ensemble of statistical downscaling methods over Europe: Results from the
1213 VALUE perfect predictor cross-validation experiment, *International Journal of Climatology*, 39, 3750–3785,
1214 <https://doi.org/10.1002/joc.5462>, 2019.

1215 Hanssen-Bauer, I., Benestad, R.E., Lutz, J., Vikhamar-Schuler, D., Svyashchennikov, P. and Førland, E.J: Comparative
1216 Analyses of Local Historical and Future Climate Conditions Important for Reindeer Herding in Finnmark, Norway and the
1217 Yamal Nenets Autonomous Okrug, Russia. In: Mathiesen, S.D., Eira, I.M.G., Turi, E.I., Oskal, A., Pogodaev, M., Tonkopeeva,
1218 M. (eds) *Reindeer Husbandry*. Springer Polar Sciences. Springer, Cham. https://doi.org/10.1007/978-3-031-17625-8_8, 2022

1219 Hanssen-Bauer, I., E.J.Førland, I.Haddeland, H.Hisdal, S.Mayer, A.Nesje, J.E.Ø.Nilsen, S.Sandven, A.B.Sandø, A.Sorteberg
1220 og B.Ådlandsvik, *Klima i Norge 2100 – Kunnskapsgrunnlag for klimatilpasning oppdatert i 2015*. Norsk Klimaservicesenter,
1221 NCCS Report 2/2015 203pp. ISSN: 2387-3027, 2015.

1222 Hawkins, E. and Sutton, R.: The potential to narrow uncertainty in projections of regional precipitation change, *Clim Dyn*, 37,
1223 407–418, <https://doi.org/10.1007/s00382-010-0810-6>, 2011.

1224 [Hersbach, H., Bell, B., Berrisford, P., Hirahara, S., Horányi, A., Muñoz-Sabater, J., Nicolas, J., Peubey, C., Radu, R., Schepers,](#)
1225 [D., Simmons, A., Soci, C., Abdalla, S., Abellan, X., Balsamo, G., Bechtold, P., Biavati, G., Bidlot, J., Bonavita, M., De Chiara,](#)
1226 [G., Dahlgren, P., Dee, D., Diamantakis, M., Dragani, R., Flemming, J., Forbes, R., Fuentes, M., Geer, A., Haimberger, L.,](#)
1227 [Healy, S., Hogan, R. J., Hólm, E., Janisková, M., Keeley, S., Laloyaux, P., Lopez, P., Lupu, C., Radnoti, G., de Rosnay, P.,](#)
1228 [Rozum, I., Vamborg, F., Villaume, S., and Thépaut, J.-N.: The ERA5 global reanalysis. *Quarterly Journal of the Royal*](#)
1229 [Meteorological Society](#), 146, 1999–2049, <https://doi.org/10.1002/qj.3803>, 2020.

1230 Hisdal, H., Vikhamar-Schuler, D., Førland, E., and Nilsen, I. (2021). Klimaprofiler for fylker. (“Climate factsheets for
1231 counties”). NCCS Report 2/2021, Norwegian Centre for Climate Services, Oslo, Norway. (In Norwegian).
1232 https://klimaservicesenter.no/kss/rapporter/rapporter-og-publikasjoner_2

1233 Huang, S., Eisner, S., Magnusson, J. O., Lussana, C., Yang, X., and Beldring, S.: Improvements of the spatially distributed
1234 hydrological modelling using the HBV model at 1 km resolution for Norway, *Journal of Hydrology*, 577, 123585,
1235 <https://doi.org/10.1016/j.jhydrol.2019.03.051>, 2019.

1236 Huang, S., Eisner, S., Haddeland, I., and Tadege Mengistu, Z.: Evaluation of two new-generation global soil databases for
1237 macro-scale hydrological modelling in Norway, *Journal of Hydrology*, 610, 127895,
1238 <https://doi.org/10.1016/j.jhydrol.2022.127895>, 2022.

Feltkode endret

1239 [Huang, S., Eisner, S., Wong, W. K., and Cattaneo, N.: The potential impacts of climate and forest changes on streamflow for](#)
1240 [micro-, meso- and macro-scale catchments in Norway, *Journal of Hydrology: Regional Studies*, 57, 102147,](#)
1241 <https://doi.org/10.1016/j.ejrh.2024.102147>, 2025a.

formaterte: Engelsk (USA)

1242 Huang, S., Haddeland, I., Lussana, C., Dobler, A., and Tveito, O.E.: Daily climate and hydrological reference data for Norway
1243 [Data set]. Dataset published 2025 via Norwegian Meteorological Institute, <https://doi.org/10.21343/gbq0-497>, 2025b.

1244 [Huang, S., Wong, W.K., Tveito, O.E., Haddeland, I.: Impacts of empirical and physical evaporation methods on changes in](#)
1245 [hydrological components and drought indices under climate change scenarios, *Hydrology Research*, doi: 10.2166/nh.2026.220,](#)
1246 [2026.](#)

1247 Hundecha, Y., Sunyer, M. A., Lawrence, D., Madsen, H., Willems, P., Bürger, G., Kriaučiūnienė, J., Loukas, A., Martinkova,
1248 M., Osuch, M., Vasiliades, L., von Christerson, B., Vormoor, K., and Yücel, I.: Inter-comparison of statistical downscaling
1249 methods for projection of extreme flow indices across Europe, *Journal of Hydrology*, 541, 1273–1286,
1250 <https://doi.org/10.1016/j.jhydrol.2016.08.033>, 2016.

1251 Huss, M., Jouviet, G., Farinotti, D., and Bauder, A.: Future high-mountain hydrology: a new parameterization of glacier retreat,
1252 *Hydrology and Earth System Sciences*, 14, 815–829, <https://doi.org/10.5194/hess-14-815-2010>, 2010.

1253 [Hübener, H., Hoffmann, P., Keuler, K., Pfeifer, S., Ramthun, H., Spekat, A., Steger, C., and Warrach-Sagi, K.: Deriving user-](#)
1254 [informed climate information from climate model ensemble results, in: *Advances in Science and Research, 16th EMS Annual*](#)
1255 [Meeting & 11th European Conference on Applied Climatology \(ECAC\) -, 261–269, <https://doi.org/10.5194/asr-14-261-2017>,](#)
1256 [2017.](#)

formaterte: Engelsk (USA)

1257 IPCC: Climate Change 2021: The Physical Science Basis. Contribution of Working Group I to the Sixth Assessment Report
1258 of the Intergovernmental Panel on Climate Change[Masson-Delmotte, V., P. Zhai, A. Pirani, S.L. Connors, C. Péan, S. Berger,
1259 N. Caud, Y. Chen, L. Goldfarb, M.I. Gomis, M. Huang, K. Leitzell, E. Lonnoy, J.B.R. Matthews, T.K. Maycock, T. Waterfield,
1260 O. Yelekçi, R. Yu, and B. Zhou (eds.)]. Cambridge University Press, Cambridge, United Kingdom and New York, NY, USA,
1261 In press, doi:10.1017/9781009157896, 2021.

1262 Jacob, D., Petersen, J., Eggert, B., Alias, A., Christensen, O. B., Bouwer, L. M., Braun, A., Colette, A., Déqué, M., Georgievski,
1263 G., Georgopoulou, E., Gobiet, A., Menut, L., Nikulin, G., Haensler, A., Hempelmann, N., Jones, C., Keuler, K., Kovats, S.,
1264 Kröner, N., Kotlarski, S., Kriegsmann, A., Martin, E., van Meijgaard, E., Moseley, C., Pfeifer, S., Preuschmann, S.,
1265 Radermacher, C., Radtke, K., Rechid, D., Rounsevell, M., Samuelsson, P., Somot, S., Soussana, J.-F., Teichmann, C.,
1266 Valentini, R., Vautard, R., Weber, B., and Yiou, P.: EURO-CORDEX: new high-resolution climate change projections for
1267 European impact research, *Reg Environ Change*, 14, 563–578, <https://doi.org/10.1007/s10113-013-0499-2>, 2014.

1268 Jacob, D., Teichmann, C., Sobolowski, S., Katragkou, E., Anders, I., Belda, M., Benestad, R., Boberg, F., Buonomo, E.,
1269 Cardoso, R. M., Casanueva, A., Christensen, O. B., Christensen, J. H., Coppola, E., De Cruz, L., Davin, E. L., Dobler, A.,
1270 Domínguez, M., Fealy, R., Fernandez, J., Gaertner, M. A., García-Díez, M., Giorgi, F., Gobiet, A., Goergen, K., Gómez-
1271 Navarro, J. J., Alemán, J. J. G., Gutiérrez, C., Gutiérrez, J. M., Güttler, I., Haensler, A., Halenka, T., Jerez, S., Jiménez-
1272 Guerrero, P., Jones, R. G., Keuler, K., Kjellström, E., Knist, S., Kotlarski, S., Maraun, D., van Meijgaard, E., Mercogliano, P.,
1273 Montávez, J. P., Navarra, A., Nikulin, G., de Noblet-Ducoudré, N., Panitz, H.-J., Pfeifer, S., Piazza, M., Pichelli, E.,
1274 Pietikäinen, J.-P., Prein, A. F., Preuschmann, S., Rechid, D., Rockel, B., Romera, R., Sánchez, E., Sieck, K., Soares, P. M. M.,
1275 Somot, S., Srncic, L., Sørland, S. L., Termonia, P., Truhetz, H., Vautard, R., Warrach-Sagi, K., and Wulfmeyer, V.: Regional
1276 climate downscaling over Europe: perspectives from the EURO-CORDEX community, *Reg Environ Change*, 20, 51,
1277 <https://doi.org/10.1007/s10113-020-01606-9>, 2020.

1278 Katragkou, E., Sobolowski, S.P., Teichmann, C., Solmon, F., Pavlidis, V., Rechid, D., Hoffmann, P., Fernández, J., Nikulin,
1279 G. and Jacob, D.: Delivering an improved framework for the new generation of CMIP6-driven EURO-CORDEX regional
1280 climate simulations. *Bulletin of the American Meteorological Society*, 105(6), pp.E962-E974, [https://doi.org/10.1175/BAMS-](https://doi.org/10.1175/BAMS-D-23-0131.1)
1281 [D-23-0131.1](https://doi.org/10.1175/BAMS-D-23-0131.1), 2024.

1282 *Kay, A. L.: A comparison of hydrological impacts from two ensembles of regional climate projections with a range of climate*
1283 *sensitivities, Reg Environ Change, 25, 89, https://doi.org/10.1007/s10113-025-02426-5, 2025,*

1284 Kundzewicz, Z. W., Krysanova, V., Dankers, R., Hirabayashi, Y., Kanae, S., Hattermann, F. F., Huang, S., Milly, P. C. D.,
1285 Stoffel, M., Driessen, P. P. J., Matczak, P., Quevauviller, P., and Schellnhuber, H.-J.: Differences in flood hazard projections
1286 in Europe – their causes and consequences for decision making, *Hydrological Sciences Journal*, 62, 1–14,
1287 <https://doi.org/10.1080/02626667.2016.1241398>, 2017.

1288 Kuya, E. K., Hanssen-Bauer, I., Mayer, S., and Heiberg, H.: Projected changes of rain, sleet, and snowfall in Norway, *Norsk*
1289 *Geografisk Tidsskrift - Norwegian Journal of Geography*, 78, 73–87, <https://doi.org/10.1080/00291951.2024.2360409>, 2024.

1290 Lafferty, D. C. and Srivier, R. L.: Downscaling and bias-correction contribute considerable uncertainty to local climate
1291 projections in CMIP6, *npj Clim Atmos Sci*, 6, 158, <https://doi.org/10.1038/s41612-023-00486-0>, 2023.

1292 Lawrence, D.: Uncertainty introduced by flood frequency analysis in projections for changes in flood magnitudes under a
1293 future climate in Norway. *Journal of Hydrology: Regional Studies* 28:100675, <https://doi.org/10.1016/j.ejrh.2020.100675>,
1294 2020.

formaterte: Engelsk (USA)

1295 Li, H., Beldring, S., Xu, C.-Y., Huss, M., Melvold, K., and Jain, S. K.: Integrating a glacier retreat model into a hydrological
1296 model – Case studies of three glacierised catchments in Norway and Himalayan region, *Journal of Hydrology*, 527, 656–667,
1297 <https://doi.org/10.1016/j.jhydrol.2015.05.017>, 2015.

1298 Li, L., Wang, B., Feng, P., Jägermeyr, J., Asseng, S., Müller, C., Macadam, I., Liu, D. L., Waters, C., Zhang, Y., He, Q., Shi,
1299 Y., Chen, S., Guo, X., Li, Y., He, J., Feng, H., Yang, G., Tian, H., and Yu, Q.: The optimization of model ensemble composition
1300 and size can enhance the robustness of crop yield projections, *Commun Earth Environ*, 4, 362, <https://doi.org/10.1038/s43247-023-01016-9>, 2023.

1301

1302 [Liersch, S., Drews, M., Pilz, T., Salack, S., Sietz, D., Aich, V., A D Larsen, M., Gädeke, A., Halsnæ s, K., Thiery, W., Huang, S., Lobanova, A., Koch, H., and Hattermann, F. F.: One simulation, different conclusions—the baseline period makes the difference!, *Environ. Res. Lett.*, 15, 104014, <https://doi.org/10.1088/1748-9326/aba3d7>, 2020.](#)

1303

1304

1305 Lussana, C.: seNorge observational gridded datasets, MET report 7-2020, https://www.met.no/publikasjoner/met-report/met-report-2020/_attachment/download/9f79d391-62d8-4fc1-a61a-9f0e7f1de389:8c74ebf2118593aa75272e6aff416ce66f86e73f/MET-report-07-2020.pdf, 2020.

1306

1307

1308 Lussana, C., Tveito, O. E., Dobler, A., and Tunheim, K.: seNorge_2018, daily precipitation, and temperature datasets over
1309 Norway, *Earth System Science Data*, 11, 1531–1551, <https://doi.org/10.5194/essd-11-1531-2019>, 2019.

1310

1311 Lutz, J., Hanssen-Bauer, I., Tveito, O. E. and Dobler, A.: Precipitation variability in Norway 1961–2020. MET-report 01-
1312 2024, https://www.met.no/publikasjoner/met-report/_attachment/download/f5ba4d69-dba2-4eb6-bed9-0189178b5e7a:ba4f4974e503f9509d33f101efc40145b47a59e6/MET%20report%201%202024.pdf, 2024.

1313

1314 Majasalmi, T., Eisner, S., Astrup, R., Fridman, J., and Bright, R. M.: An enhanced forest classification scheme for modeling
1315 vegetation–climate interactions based on national forest inventory data, *Biogeosciences*, 15, 399–412,
<https://doi.org/10.5194/bg-15-399-2018>, 2018.

1316

1317 [Maraun, D.: Bias Correction, Quantile Mapping, and Downscaling: Revisiting the Inflation Issue. *Journal of Climate*, 26, 2137–2143. <https://doi.org/10.1175/jcli-d-12-00821.1>, 2013.](#)

1318

1319 [Maraun, D. and Widmann, M.: *Statistical Downscaling and Bias Correction for Climate Research*. Cambridge University Press, 347 pp, 2018.](#)

1320

1321 Martinich, J. and Crimmins, A.: Climate damages and adaptation potential across diverse sectors of the United States, *Nature Climate Change*, 9, 397–404, 2019.

1322

1323 [Matiu, M., Napoli, A., Kotlarski, S., Zardi, D., Bellin, A., and Majone, B.: Elevation-dependent biases of raw and bias-adjusted EURO-CORDEX regional climate models in the European Alps, *Climate Dynamics*, <https://doi.org/10.1007/s00382-024-07376-y>, 2024.](#)

1324

formaterte: Norsk (bokmål)

formaterte: Norsk (bokmål)

formaterte: Norsk (bokmål)

formaterte: Norsk (bokmål)

Feltkode endret

Feltkode endret

formaterte: Norsk (bokmål)

formaterte: Engelsk (USA)

1325 Mayer, S., Khasandi Kuya, E., Antonsen, K., Abegg, B., and Hanssen-Bauer, I.: Warmer and wetter: Outlining climate services
1326 for snow-dependent tourism in Norway – The case of Lofoten, *Climate Services*, 32, 100405,
1327 <https://doi.org/10.1016/j.cliser.2023.100405>, 2023.

1328 McAfee, S. A.: Methodological differences in projected potential evapotranspiration, *Climatic Change*, 120, 915–930,
1329 <https://doi.org/10.1007/s10584-013-0864-7>, 2013.

1330 ~~Maraun, D. and Widmann, M.: *Statistical Downscaling and Bias Correction for Climate Research*. Cambridge University
1331 Press, 347 pp, 2018.~~

1332 McSweeney, C. F., Jones, R. G., Lee, R. W., and Rowell, D. P.: Selecting CMIP5 GCMs for downscaling over multiple
1333 regions, *Clim Dyn*, 44, 3237–3260, <https://doi.org/10.1007/s00382-014-2418-8>, 2015.

1334 Mehrotra, R. and Sharma, A.: A Resampling Approach for Correcting Systematic Spatiotemporal Biases for Multiple Variables
1335 in a Changing Climate, *Water Resources Research*, 55, 754–770, <https://doi.org/10.1029/2018WR023270>, 2019.

1336 Meyer, J., Kohn, I., Stahl, K., Hakala, K., Seibert, J., and Cannon, A. J.: Effects of univariate and multivariate bias correction
1337 on hydrological impact projections in alpine catchments, *Hydrol. Earth Syst. Sci.*, 23, 1339–1354, [https://doi.org/10.5194/hess-](https://doi.org/10.5194/hess-23-1339-2019)
1338 [23-1339-2019](https://doi.org/10.5194/hess-23-1339-2019), 2019.

1339 Moriasi, D. N., Arnold, J. G., Liew, M. W. V., Bingner, R. L., Harmel, R. D., and Veith, T. L.: Model Evaluation Guidelines
1340 for Systematic Quantification of Accuracy in Watershed Simulations, *Transactions of the ASABE*, 50, 885–900,
1341 <https://doi.org/10.13031/2013.23153>, 2007.

1342 Müller, M., Homleid, M., Ivarsson, K.-I., Køltzow, M. A. Ø., Lindskog, M., Midtbø, K. H., Andrae, U., Aspelien, T., Berggren,
1343 L., Bjørge, D., Dahlgren, P., Kristiansen, J., Randriamampianina, R., Ridal, M., and Vignes, O.: AROME-MetCoOp: A Nordic
1344 Convective-Scale Operational Weather Prediction Model, <https://doi.org/10.1175/WAF-D-16-0099.1>, 2017.

1345 Nash, J.E. and Sutcliffe, J.V.: River flow forecasting through conceptual models part I -A discussion of principles, *J Hydrol*,
1346 10, 282–290, 1970.

1347 Nilsen, I. B., Hanssen-Bauer, I., Tveito, O. E., and Wong, W. K.: Projected changes in days with zero-crossings for Norway,
1348 *International Journal of Climatology*, 41, 2173–2188, <https://doi.org/10.1002/joc.6913>, 2021.

1349 Nilsen, I. B., Hanssen-Bauer, I., Dyrddal, A. V., Hisdal, H., Lawrence, D., Haddeland, I., and Wong, W. K.: From Climate
1350 Model Output to Actionable Climate Information in Norway, *Front. Clim.*, 4, <https://doi.org/10.3389/fclim.2022.866563>,
1351 2022.

Feltkode endret

1352 Norwegian Government (2024). Statlige Planretningslinjer for klima- og energi. (“government guidelines on climate and
1353 renergy”). Available online at: <https://lovdata.no/dokument/SF/forskrift/2024-12-20-3359> (accessed December 06. October
1354 2025).

1355 Padrón, R. S., Gudmundsson, L., Decharme, B., Ducharne, A., Lawrence, D. M., Mao, J., Peano, D., Krinner, G., Kim, H.,
1356 and Seneviratne, S. I.: Observed changes in dry-season water availability attributed to human-induced climate change, *Nat.*
1357 *Geosci.*, 13, 477–481, <https://doi.org/10.1038/s41561-020-0594-1>, 2020.

1358 [Paz, S.M. and Willems, P.: Uncovering the strengths and weaknesses of an ensemble of quantile mapping methods for](#)
1359 [downscaling precipitation change in Southern Africa. *J. Hydrol. -Reg. Stud.* 41, 101104,](#)
1360 [https://doi.org/10.1016/j.ejrh.2022.101104, 2022.](#)

1361 Peter, J., Vogel, E., Sharples, W., Bende-Michl, U., Wilson, L., Hope, P., Dowdy, A., Kociuba, G., Srikanthan, S., Duong, V.
1362 C., Roussis, J., Matic, V., Khan, Z., Oke, A., Turner, M., Baron-Hay, S., Johnson, F., Mehrotra, R., Sharma, A., Thatcher, M.,
1363 Azarvinand, A., Thomas, S., Boschhat, G., Donnelly, C., and Argent, R.: Continental-scale bias-corrected climate and
1364 hydrological projections for Australia, *Geoscientific Model Development*, 17, 2755–2781, [https://doi.org/10.5194/gmd-17-](https://doi.org/10.5194/gmd-17-2755-2024)
1365 [2755-2024](#), 2024.

1366 Pirk, N., Aalstad, K., Yilmaz, Y. A., Vatne, A., Popp, A. L., Horvath, P., Bryn, A., Vollsnes, A. V., Westermann, S., Berntsen,
1367 T. K., Stordal, F., and Tallaksen, L. M.: Snow–vegetation–atmosphere interactions in alpine tundra, *Biogeosciences*, 20, 2031–
1368 2047, <https://doi.org/10.5194/bg-20-2031-2023>, 2023.

1369 Pourmokhtarian, A., Driscoll, C. T., Campbell, J. L., Hayhoe, K., and Stoner, A. M. K.: The effects of climate downscaling
1370 technique and observational data set on modeled ecological responses, *Ecological Applications*, 26, 1321–1337,
1371 <https://doi.org/10.1890/15-0745>, 2016.

1372 Reistad, M., Øyvind Breivik, Haakenstad, H., Aarnes, O. J., Furevik, B. R., and Bidlot, J.-R.: A high-resolution hindcast of
1373 wind and waves for the North Sea, the Norwegian Sea, and the Barents Sea, *J. Geophys. Res.*, 116,
1374 <https://doi.org/10.1029/2010JC006402>, 2011.

1375 Reyniers, N., Zha, Q., Addor, N., Osborn, T. J., Forstnhäusler, N., and He, Y.: Two sets of bias-corrected regional UK Climate
1376 Projections 2018 (UKCP18) of temperature, precipitation and potential evapotranspiration for Great Britain, *Earth System*
1377 *Science Data*, 17, 2113–2133, <https://doi.org/10.5194/essd-17-2113-2025>, 2025.

1378 Rössler, O., Fischer, A. M., Huebener, H., Maraun, D., Benestad, R. E., Christodoulides, P., Soares, P. M. M., Cardoso, R. M.,
1379 Pagé, C., Kanamaru, H., Kreienkamp, F., and Vlachogiannis, D.: Challenges to link climate change data provision and user

1380 needs: Perspective from the COST-action VALUE, International Journal of Climatology, 39, 3704–3716,
1381 <https://doi.org/10.1002/joc.5060>, 2019.

1382 Statistics Norway: [Land use and land cover – SSB](#), last accessed on 27.03.2025, [2025](#).

1383 Schumacher, D.L., Singh, J., Hauser, M., Fischer, E.M., Wild, M. and Seneviratne, S.I.: Exacerbated summer European
1384 warming not captured by climate models neglecting long-term aerosol changes. Communications Earth & Environment, 5(1),
1385 p.182, <https://doi.org/10.1038/s43247-024-01332-8>, 2024.

1386 [Sobolowski, S., Somot, S., Fernandez, J., Evin, G., Brands, S., Maraun, D., Kotlarski, S., Jury, M., Benestad, R.E., Teichmann,](#)
1387 [C. and Christensen, O.B.: GCM Selection and Ensemble Design: Best Practices and Recommendations from the EURO-](#)
1388 [CORDEX Community. Bulletin of the American Meteorological Society, 106\(9\), pp.E1834-E1850.](#)
1389 <https://doi.org/10.1175/BAMS-D-23-0189.1>, 2025.

1390 Tam, B., Bonsal, B., Zhang, X., Zhang, Q., and Rong, R.: Assessing Potential Evapotranspiration Methods in Future Drought
1391 Projections across Canada, Atmosphere-Ocean, 62, 193–205, <https://doi.org/10.1080/07055900.2023.2288632>, 2024.

1392 Tang, J., Niu, X., Wang, S., Gao, H., Wang, X., and Wu, J.: Statistical downscaling and dynamical downscaling of regional
1393 climate in China: Present climate evaluations and future climate projections, Journal of Geophysical Research: Atmospheres,
1394 121, 2110–2129, <https://doi.org/10.1002/2015JD023977>, 2016.

1395 Taylor, K. E., Stouffer, R. J., and Meehl, G. A.: An overview of CMIP5 and the experiment design, B. Am. Meteorol. Soc.,
1396 93, 485–498, <https://doi.org/10.1175/BAMS-D-11-00094.1>, 2012.

1397 ~~Taylor, K. E., Stouffer, R. J., and Meehl, G. A.: An Overview of CMIP5 and the Experiment Design,~~
1398 ~~<https://doi.org/10.1175/BAMS-D-11-00094.1>, 2012.~~

1399 Thorarinsdottir, T. L., Gneiting, T., and Gissibl, N.: Using proper divergence functions to evaluate climate models. SIAM-
1400 ASA J. Uncertainty Quantif., 1, 522–534, <https://doi.org/10.1137/130907550>, 2013.

1401 [Tong, Y., Gao, X., Han, Z., Xu, Y. and Giorgi, F.: Bias correction of temperature and precipitation over China for RCM](#)
1402 [simulations using the QM and QDM methods, Climate Dynamics 57, 1425-1443, https://doi.org/10.1007/s00382-020-05447-](#)
1403 [4, 2021.](#)

1404 Tveito, O. E.: Norwegian standard climate normals 1991-2020 – the methodological approach, MET report 5 2021,
1405 [69](https://www.met.no/publikasjoner/met-report/met-report-2021/_/attachment/download/31bb0160-d8cf-4a2b-9646-</p></div><div data-bbox=)

1406 4df6f5904059:3ac4fec6cf3fb7919ae42db2b63ad8e8b9e6a6/METreport%2005_2021_New_Norwegian_standard_climate_
1407 normals_1991_2020-signert.pdf, 2021.

1408 Vautard, R., Kadyrov, N., Iles, C., Boberg, F., Buonomo, E., Bülow, K., Coppola, E., Corre, L., van Meijgaard, E.,
1409 Nogherotto, R., Sandstad, M., Schwingshackl, C., Somot, S., Aalbers, E., Christensen, O. B., Ciarlo, J. M., Demory, M.-E.,
1410 Giorgi, F., Jacob, D., Jones, R. G., Keuler, K., Kjellström, E., Lenderink, G., Levavasseur, G., Nikulin, G., Sillmann, J.,
1411 Solidoro, C., Sørland, S. L., Steger, C., Teichmann, C., Warrach-Sagi, K., and Wulfmeyer, V.: Evaluation of the Large EURO-
1412 CORDEX Regional Climate Model Ensemble, *Journal of Geophysical Research: Atmospheres*, 126, e2019JD032344,
1413 <https://doi.org/10.1029/2019JD032344>, 2021.

1414 [Vetter, T., Reinhardt, J., Flörke, M., van Griensven, A., Hattermann, F., Huang, S., Koch, H., Pechlivanidis, I. G., Plötner, S.,](#)
1415 [Seidou, O., Su, B., Vervoort, R. W., and Krysanova, V.: Evaluation of sources of uncertainty in projected hydrological changes](#)
1416 [under climate change in 12 large-scale river basins. *Climatic Change*, 141, 419–433. \[https://doi.org/10.1007/s10584-016-1794-\]\(https://doi.org/10.1007/s10584-016-1794-y\)](#)
1417 [y, 2017.](#)

1418 Wang, X. and Liu, L.: The Impacts of Climate Change on the Hydrological Cycle and Water Resource Management, *Water*,
1419 15, 2342, <https://doi.org/10.3390/w15132342>, 2023.

1420 [Wilkinson, M. D., Dumontier, M., Aalbersberg, Ij. J., Appleton, G., Axton, M., Baak, A., Blomberg, N., Boiten, J.-W., da](#)
1421 [Silva Santos, L. B., Bourne, P. E., Bouwman, J., Brookes, A. J., Clark, T., Crosas, M., Dillo, I., Dumon, O., Edmunds, S.,](#)
1422 [Evelo, C. T., Finkers, R., Gonzalez-Beltran, A., Gray, A. J. G., Groth, P., Goble, C., Grethe, J. S., Heringa, J., 't Hoen, P. A.](#)
1423 [C., Hoofi, R., Kuhn, T., Kok, R., Kok, J., Lusher, S. J., Martone, M. E., Mons, A., Packer, A. L., Persson, B., Rocca-Serra, P.,](#)
1424 [Roos, M., van Schaik, R., Sansone, S.-A., Schultes, E., Sengstag, T., Slater, T., Strawn, G., Swertz, M. A., Thompson, M., van](#)
1425 [der Lei, J., van Mulligen, E., Velterop, J., Waagmeester, A., Wittenburg, P., Wolstencroft, K., Zhao, J., and Mons, B.: The](#)
1426 [FAIR Guiding Principles for scientific data management and stewardship. *Sci Data*, 3, 160018.](#)
1427 <https://doi.org/10.1038/sdata.2016.18>, 2016.

1428 Wolff, M. A., Isaksen, K., Petersen-Øverleir, A., Ødemark, K., Reitan, T., and Brækkan, R.: Derivation of a new continuous
1429 adjustment function for correcting wind-induced loss of solid precipitation: results of a Norwegian field study, *Hydrology and*
1430 *Earth System Sciences*, 19, 951–967, <https://doi.org/10.5194/hess-19-951-2015>, 2015.

1431 Wong, W.K., Dobler, A., Huang, S., Beldring, S., Melvold, K., Ruan, G.: Daily bias-adjusted climate (COR-BA-2025) and
1432 hydrological (distHBV-COR-BA-2025) projections for Norway [Data set]. Dataset published 2025 via Norwegian
1433 Meteorological Institute <https://doi.org/10.21343/0k90-6w67>, 2025

formaterte: Engelsk (USA)

1434 Wong, W.K., Haddeland, I., Lawrence, D., and Beldring, S.: Gridded 1x1 km climate and hydrological projections for Norway.
1435 NVE Report No. 59, Norwegian Water Resources and Energy Directorate, Oslo, Norway, 2016.

1436 Yilmaz, K. K., Gupta, H. V., and Wagener, T.: A process-based diagnostic approach to model evaluation: Application to the
1437 NWS distributed hydrologic model, *Water Resources Research*, 44, <https://doi.org/10.1029/2007WR006716>, 2008.

1438 Yuan, Q., Thorarinsdottir, T. L., Beldring, S., Wong, W. K., Huang, S., and Xu, C.-Y.: New Approach for Bias Correction and
1439 Stochastic Downscaling of Future Projections for Daily Mean Temperatures to a High-Resolution Grid, *J. Appl. Meteorol.*
1440 *Clim.*, 58, 2617–2632, <https://doi.org/10.1175/JAMC-D-19-0086.1>, 2019.

1441 Yuan Q., Thorarinsdottir T.L., Beldring S., Wong W.K., and Xu C.-Y.: Bridging the scale gap: obtaining high-resolution
1442 stochastic simulations of gridded daily precipitation in a future climate, *Hydrol. Earth Syst. Sci.*, 25 (9), pp. 5259-5275,
1443 <https://doi.org/10.5194/hess-25-5259-2021>, 2021.

1444 [Zhang, H., Chapman, S., Trancoso, R., Toombs, N. and Syktus, J.: Assessing the impact of bias correction approaches on
1445 climate extremes and the climate change signal, *Meteorol. Appl.*, 31, 1-18, <https://doi.org/10.1002/met.2204>, 2024.](https://doi.org/10.1002/met.2204)

1446 Zhang, L., Xu, Y., Meng, C., Li, X., Liu, H., and Wang, C.: Comparison of Statistical and Dynamic Downscaling Techniques
1447 in Generating High-Resolution Temperatures in China from CMIP5 GCMs, <https://doi.org/10.1175/JAMC-D-19-0048.1>,
1448 2020.

1449